Atmos. Chem. Phys. Discuss., doi:10.5194/acp-2016-1032, 2016
Manuscript under review for journal Atmos. Chem. Phys.
Published: 29 November 2016

Atmospheric Chemistry and Physics Discussions

Source attribution of black carbon and its direct radiative forcing in China

Yang Yang[1], Hailong Wang[1*], Steven J. Smith[2], Po-Lun Ma[1], Philip J. Rasch[1]

[1]Atmospheric Science and Global Change Division, Pacific Northwest National Laboratory, Richland, Washington, USA
[2]Joint Global Change Research Institute, Pacific Northwest National Laboratory, College Park, Maryland, USA

*Correspondence to yang.yang@pnnl.gov and hailong.wang@pnnl.gov

Atmos. Chem. Phys. Discuss., doi:10.5194/acp-2016-1032, 2016
Manuscript under review for journal Atmos. Chem. Phys.
Published: 29 November 2016

Atmospheric Chemistry and Physics Discussions

Abstract

The source attributions for mass concentration, haze formation, transport, and direct radiative forcing of black carbon (BC) in various regions of China are quantified in this study using the Community Earth System Model (CESM) with a source-tagging technique. Anthropogenic emissions are from the Community Emissions Data System that is newly developed for the Coupled Model Intercomparison Project Phase 6 (CMIP6). Over North China where the air quality is often poor, about 90% of near-surface BC concentration is contributed by local emissions. 30% of BC concentration over South China in winter can be attributed to emissions from North China and 10% comes from sources outside China in spring. For other regions in China, BC is largely contributed from non-local sources. We further investigated potential factors that contribute to the poor air quality in China. During polluted days, a net inflow of BC transported from non-local source regions associated with anomalous winds plays an important role in increasing local BC concentrations. BC-containing particles emitted from East Asia can also be transported across the Pacific. Our model results show that emissions from inside and outside China are equally important for the BC outflow from East Asia, while emissions from China account for 7% of BC concentration and 25% in column burden in western United States in spring. Radiative forcing estimated shows that 66% of the annual mean BC direct radiative forcing (2.3 W m^{-2}) in China results from local emissions, and the remaining 34% are contributed by emissions outside of China. Efficiency analysis shows that reduction in BC emissions over eastern China could benefit more on the regional air quality in China, especially in winter haze season.

Atmos. Chem. Phys. Discuss., doi:10.5194/acp-2016-1032, 2016
Manuscript under review for journal Atmos. Chem. Phys.
Published: 29 November 2016

Atmospheric Chemistry and Physics Discussions

1. Introduction

Black carbon (BC), as a component of atmospheric fine particulate matter ($PM_{2.5}$), is harmful to human health (Anenberg et al., 2011; Janssen et al., 2012). In addition to its impact on air quality, as the most efficient light-absorbing anthropogenic aerosols, BC is thought to exert a substantial influence on climate (Bond et al., 2013; IPCC, 2013; Liao et al., 2015). It can heat the atmosphere through absorbing solar radiation (Ramanathan and Carmichael, 2008), influence cloud microphysical and dynamical processes (Jacobson, 2006; McFarquhar and Wang, 2006), and reduce surface albedo through deposition on snow and ice (Flanner et al., 2007; Qian et al., 2015).

Due to accelerated urbanization and rapid economic growth, emissions of BC in China increased dramatically during recent decades. It contributed to about one fourth of the global emissions of BC in recent decades (Bond et al., 2007). Strong emissions lead to high concentrations of BC over China. Zhang et al. (2008) collected aerosol samples at 18 stations spread over China during 2006 and reported BC concentrations in a range of 9–14 μg m^{-3} at urban sites, 2–5 μg m^{-3} at rural sites, and about 0.35 μg m^{-3} at remote background sites. BC also exerts significant positive direct radiative forcing (DRF) at the top of the atmosphere (TOA) in China. Using the Regional Climate Chemistry Modeling System (RegCCMs), Zhuang et al. (2013) reported an annual mean BC DRF of 2–5 W m^{-2} at TOA over eastern China and about 6 W m^{-2} over Sichuan Basin in year 2006. Li et al. (2016) also showed a strong DRF of BC over the North China Plain and Sichuan Basin in most seasons except for spring when the strongest BC DRF with values of 4–6 W m^{-2} shifted to southern China.

BC is the product of incomplete combustion of fossil fuels, biofuels, and open burning, such as forest and grassland fires and agricultural waste burning on fields. In the atmosphere the average lifetime of BC is only a few days, due to both wet removal and dry deposition, which is much shorter than that of long-lived greenhouse gases. In addition, BC lifetime is region dependent. BC in East Asia has a shorter lifetime than the global mean value due to a faster regional removal (H. Wang et al.,

Atmos. Chem. Phys. Discuss., doi:10.5194/acp-2016-1032, 2016
Manuscript under review for journal Atmos. Chem. Phys.
Published: 29 November 2016

Atmospheric Chemistry and Physics Discussions

2014). BC emission reductions may benefit both mitigation of global climate change and regional air quality (Shindell et al., 2012; Bond et al., 2013; Smith and Mizrahi, 2013), especially in East Asia where fuel combustion emits substantial BC along with other pollutant species. Many previous observational and/or modeling studies have examined the source sector contributions of BC over China (Zhuang et al., 2014; Y.-L. Zhang et al., 2015; Li et al., 2016). They found that residential heating and industry sectors were the largest contributors to BC concentrations in China, while biomass burning emissions from outside China were important to BC in western China. An effective BC reduction in a receptor region would require knowing not only the source sector that contributes the most to BC levels, but also the source contributions from various locations within and outside the region. However, very few previous studies have focused on the source attribution of BC concentrations in various regions of China. Li et al. (2016) examined the contributions of emissions inside and outside China to BC over China (with only two source regions) but did not divide the source contributions from different regions inside China.

Pollution levels also show substantial daily to weekly variation. In recent years, extreme wintertime hazy conditions occurred frequently in China and caused serious air pollution, affecting more than half of the 1.3 billion people (Ding and Liu, 2014). During one winter haze episode in 2013, BC concentrations increased up to about 20 and 8 μg m^{-3} in Xi'an and Beijing over northern China, and 6 and 4 μg m^{-3} in Guangzhou and Shanghai over southern China, respectively (Y.-L. Zhang et al., 2015). The transport of pollutants from upwind was reported to be one of the most important contributors to local high aerosol concentrations during haze days (L. T. Wang et al., 2014; Y. Yang et al., 2016). L. T. Wang et al. (2014) found that emissions from northern Hebei and Beijing-Tianjin were the major contributor to particulate matter ($PM_{2.5}$) pollution in Shijiazhuang in January 2013. Yang et al. (2016) confirmed a connection between wind fields and $PM_{2.5}$ concentrations during winter hazy days through model simulations and statistical analysis. They also found that weakened winds contributed to increases in winter aerosol concentrations and hazy days over eastern China during recent decades. As a chemically inert species, atmospheric BC

Atmos. Chem. Phys. Discuss., doi:10.5194/acp-2016-1032, 2016
Manuscript under review for journal Atmos. Chem. Phys.
Published: 29 November 2016

is a good tracer to investigate the source region contributions from local and non-local emissions during polluted conditions that are related to long-range transport.

BC particles originating from East Asia can also be transported across the North Pacific, reaching North America (Hadley et al., 2007; Ma et al., 2013a; Matsui et al., 2013; H. Wang et al., 2014; Yang et al., 2015). Matsui et al. (2013) simulated outflow of BC from East Asia using the Community Multiscale Air Quality (CMAQ) model and found that anthropogenic emissions from China, biomass burning emissions from Southeast Asia, and biomass burning emissions from Siberia and Kazakhstan contributed 61%, 17%, and 6%, respectively, to the eastward BC flux at 150°E averaged over 2008–2010. Hadley et al. (2007) estimated the trans-Pacific transport of BC during April of 2004 using the Chemical Weather Forecast System (CFORS) model and reported that, across 130°W, 75% of BC transported into North America originated from Asia. Huang et al. (2012) simulated BC using the Sulfur Transport and Deposition Model (STEM), and found emissions outside North America contributed to 30–80% of column BC over North America in summer 2008. H. Wang et al. (2014) examined the long-term (1995-2005) average global source-receptor relationship of BC and found that BC emitted from the entire East Asia only contribute less than 5% to the total BC burden in North America, although the contribution is up to 40% near the west coast region. Few studies have examined the outflow from East Asia and inflow into North America contributed from source regions in and outside China. In addition, the emissions of BC from China increased dramatically during the last few years, with the annual total anthropogenic emissions estimated to have almost doubled in year 2014 compared to year 2000, shown in the newly developed Community Emissions Data System (CEDS; Hoesly et al. 2016). Therefore, the long-range transport of BC and source-receptor relationships could be quite different from previous studies.

Due to its warming effect in the climate system, BC is potentially important for climate mitigation and has drawn much attention recently. Source attribution of the direct radiative effect of BC is likely to be different from that of near-surface concentration and column burden due to the dependence of radiative forcing on the

Atmos. Chem. Phys. Discuss., doi:10.5194/acp-2016-1032, 2016
Manuscript under review for journal Atmos. Chem. Phys.
Published: 29 November 2016

vertical distribution of BC and its mixing state with other species that are influenced by different regional sources. In this study, we use the Community Earth System Model (CESM) with improved representations of aerosol transport and wet removal (H. Wang et al., 2013) and a BC source-tagging technique (H. Wang et al., 2014). Anthropogenic emissions from the newly developed CEDS inventory (Hoesly et al., 2016), as released for the Coupled Model Intercomparison Project Phase 6 (CMIP6), are used to examine the source attributions for mass concentration, long-range transport, and direct radiative forcing of BC in various regions of China. We aim to quantify: (1) source region contributions to concentrations of BC over various receptor regions in China; (2) contributions to changes in BC concentrations under polluted conditions; (3) source contributions to trans-boundary and trans-Pacific transport of BC; and (4) source contributions to direct radiative forcing of BC in China.

The CESM model, emissions, and numerical experiment are described in Section 2. Section 3 provides evaluation of the simulated concentration and aerosol absorption optical depth of BC in China. Section 4 investigates source contributions to near-surface concentrations, long-range transport and direct radiative forcing of BC over various receptor regions using the BC source-tagging technique in CESM. Section 5 summarizes these results.

2. Methods

We simulate the evolution and direct radiative forcing (DRF) of BC using CESM version 1.2 (Hurrell et al., 2013). The atmospheric model in CESM is version 5 of the Community Atmosphere Model (CAM5), with horizontal grid spacing of 1.9° latitude by 2.5° longitude and 30 vertical layers ranging from the surface to 3.6 hPa used in this study. The model treats the properties and processes of major aerosol species (sea salt, mineral dust, sulfate, black carbon, primary organic matter and secondary organic aerosol) using a three-mode modal aerosol module (MAM3), in which aerosol size distributions are represented by three lognormal modes: Aitken, accumulation, and coarse modes. BC is emitted to the accumulation mode. Mass mixing ratios of different aerosol species and the number mixing ratio are predicted for each mode. A

Atmos. Chem. Phys. Discuss., doi:10.5194/acp-2016-1032, 2016
Manuscript under review for journal Atmos. Chem. Phys.
Published: 29 November 2016

more detailed description of the MAM3 representation can be found in Liu et al. (2012). The improved representations of processes related to convective transport and wet scavenging of aerosols (H. Wang et al., 2013) are also included in this newer version of the CESM/CAM5. Aerosol optical properties are parameterized in the model according to Ghan and Zaveri (2007). Besides the default total radiative fluxes calculated online, the CESM model can also calculate a separate set of radiative fluxes without considering the contribution from one or more specific components. The direct radiative forcing of those excluded species could then be calculated as the differences of these two sets of radiative fluxes (Ghan, 2013).

Anthropogenic emissions used in this study are from the CEDS dataset, as released for the CMIP6 model experiments (Hoesly et al. 2016). This newly released emission inventory includes aerosol (black carbon, organic carbon) and aerosol precursor and reactive compounds (sulfur dioxide, nitrogen oxides, ammonia, carbon monoxide, and non-methane volatile organic compounds). The emissions are provided at monthly resolution for each year of 1750–2014 on a 0.5° x 0.5° grid and include agricultural, energy, industry, residential, international shipping, solvents, surface transportation, waste treatment, and aircraft sectors. The biomass burning emissions used in this study are also developed for CMIP6 based on Global Fire Emission Database (GFED) version 4, Fire Model Intercomparison Project (FireMIP), visibility-observations and Global Charcoal Database (GCD) data (van Marle et al. 2016).

Figure 1a shows the horizontal spatial distribution of annual emissions of BC averaged over the most recent 5 years (2010–2014) and the seven geographical source regions tagged in continental China, including North China (NC), South China (SC), Southwest China (SW), Central-West China (CW), Northeast China (NE), Northwest China (NW), and Tibetan Plateau (TP). Figure 1b summarizes the total seasonal BC emissions in each of these source regions. North China has the largest annual emissions of BC in China, with maximum emission larger than 1.2 g C m^{-2} $year^{-1}$ and a regional total emission of 1089 Gg C $year^{-1}$ (44% of total emissions from continental China). Annual emissions of BC also have large values over South China

Atmos. Chem. Phys. Discuss., doi:10.5194/acp-2016-1032, 2016
Manuscript under review for journal Atmos. Chem. Phys.
Published: 29 November 2016

and Southwest China, with maximum values in the range of 0.8–1.2 g C m^{-2} $year^{-1}$, followed by Central-West China and Northeast China. Over the less economically developed Northwest China and remote region Tibetan Plateau, emissions of BC are much lower than other regions in China. The seasonal mean emissions of BC also show the same spatial pattern as the annual means. BC had the largest emissions over North China, South China, and Southwest China in all seasons, among which emissions are strongest in December-January-February (DJF), especially over North China, resulting from domestic heating. The total seasonal emissions of BC in continental China are 797, 586, 537, and 577 Gg C in DJF, March-April-May (MAM), June-July-August (JJA), and September-October-November (SON), respectively, which add up to a total annual BC emissions of 2497 Gg C averaged over years 2010–2014. The DJF emissions account for 26–35% of annual total whereas emissions in JJA only account for 17–24% over the seven source regions in continental China.

An explicit BC source tagging capability was originally implemented in CAM5 by H. Wang et al. (2014), through which emissions of BC from independent source regions and/or sectors can be explicitly tracked. This method quantifies the source–receptor relationships of BC in any receptor region within a single model simulation without perturbing emissions from individual source regions or sectors. R. Zhang et al. (2015a,b) used this method to quantify the source attributions of BC in western North America, Himalayas, and Tibetan Plateau. The same BC source tagging technique is implemented to a newer model version (CAM5.3) and applied in this study to quantify the source attributions of concentration, transport and direct radiative forcing of BC in various regions of China. BC emissions (anthropogenic plus biomass burning) from seven geographical source regions, including North China, South China, Southwest China, Central-West China, Northeast China, Northwest China, Tibetan Plateau in China, and from rest of the world (RW) are tagged. Transport and physics tendencies are calculated separately for each tagged BC in the same way as the original BC simulation in CESM. We choose the seven individual regions (North China, South China, Southwest China, Central-West China, Northeast

Atmos. Chem. Phys. Discuss., doi:10.5194/acp-2016-1032, 2016
Manuscript under review for journal Atmos. Chem. Phys.
Published: 29 November 2016

Atmospheric Chemistry and Physics Discussions

China, Northwest China, and Tibetan Plateau) and all seven regions combined (hereafter continental China) as receptor regions in this study to examine the source-receptor relationships of BC. While all emissions, including sulfur dioxides, organic carbon and BC, were used in the model simulation, tagging was only applied to BC emissions.

The CAM5 simulation is performed at 1.9° × 2.5° horizontal grid spacing using the specified-dynamics mode (Ma et al., 2013b), in which large-scale circulations (i.e., horizontal winds) are nudged to 6-hourly reanalysis data from the Modern Era Retrospective-Analysis for Research and Applications (MERRA) reanalysis data set (Rienecker et al., 2011) with a relaxation time scale of 6 hours (K. Zhang et al., 2014). The use of nudged winds allows for a more accurate simulation so that the key role of large-scale circulation patterns matches observations over the specified years. The simulation is run from year 2009 to 2014, with both time-varying aerosol emissions and meteorological fields. The first year is for spin-up and the last five years are used for analysis.

3. Model evaluation

The simulations of aerosols, especially BC, using CAM5 have been evaluated against observations including aerosol mass and number concentrations, aerosol optical properties, aerosol deposition, and cloud-nucleating properties in many previous studies (e.g., Liu et al., 2012; H. Wang et al., 2013; Ma et al., 2013b; Jiao et al., 2014; Qian et al., 2014; R. Zhang et al., 2015a,b). Here we focus on the evaluation of model performance in China using measurements of near-surface BC concentrations, aerosol index derived from satellite, and aerosol absorption optical depth from the Aerosol Robotic Network (AERONET).

3.1 Near-surface mass concentrations and column burden of BC

Figure 2 presents spatial distributions of simulated seasonal mean near-surface concentrations and column burden of BC, both of which show a similar spatial pattern to emissions of BC (Figure 1a) with the largest values over North China and the lowest values over Northwest China and Tibetan Plateau. Near-surface model results

Atmos. Chem. Phys. Discuss., doi:10.5194/acp-2016-1032, 2016
Manuscript under review for journal Atmos. Chem. Phys.
Published: 29 November 2016

are taken to be the lowest model layer (from surface to 993 hPa in average). Among all seasons, DJF has the highest BC levels, with values in the range of 6–12, 2–8, and 1–8 μg m^{-3} for near-surface concentrations and 5–9, 3–7, 2–9 mg m^{-2} for column burden over North, South, and Southwest China, respectively. In contrast, JJA has the lowest BC concentrations over China due to the lower emissions and larger wet scavenging associated with East Asian summer monsoon (Lou et al., 2016). Averaged over continental China, near-surface BC concentrations are 2.2, 1.1, 0.8, 1.3 μg m^{-3} in DJF, MAM, JJA, and SON, respectively, with seasonal variability of 38%. The column burden of BC shows smaller seasonal variability (26%), with area-weighted average of 1.9, 1.4, 1.1, and 1.3 mg m^{-2} in DJF, MAM, JJA, and SON, respectively, in China. It suggests that, besides domestic emissions in China, there are other BC sources from outside China contributing significantly to BC concentrations in the column. The magnitude, spatial distribution, and seasonal variations of simulated near-surface BC concentrations over China are similar to those in Fu et al. (2012) and X. Wang et al. (2013) using Intercontinental Chemical Transport Experiment-Phase B (INTEX-B) emission inventory (Zhang et al., 2009) and those in Li et al. (2016) using Hemispheric Transport of Air Pollution (HTAP) emission inventory (Janssens-Maenhout et al., 2015) together with a global chemical transport model.

The simulated near-surface BC concentrations are evaluated here using measurements at 14 sites of the China Meteorological Administration Atmosphere Watch Network (CAWNET) (Zhang et al., 2012). The locations of CAWNET sites are shown in Figure S1a. The observational data include monthly BC concentrations in years 2006–2007. Note that the simulated BC concentrations are for years 2010–2014. Figure 3a compares the simulated seasonal mean near-surface BC concentrations with those from CAWNET observations and Table S1 summarizes the comparison in different regions, using modeled values from the grid cell containing each observation site. Simulated BC concentrations at most sites are within the range of one third to 3 times of observed values, except for Dunhuang (94.68°E, 40.15°N) and Lhasa (91.13°E, 29.67°N) sites over western China, where BC concentrations

Atmos. Chem. Phys. Discuss., doi:10.5194/acp-2016-1032, 2016
Manuscript under review for journal Atmos. Chem. Phys.
Published: 29 November 2016

appear to be underestimated in the model (up to 20 times lower). Over North China, simulated concentrations are similar to observations in DJF, but underestimated in other seasons. Over South China, the simulations do not have large biases compared to the observed BC. However, simulated BC is underestimated in all seasons over Southwest, Central-West, Northeast, Northwest China, and Tibetan Plateau. Compared to the CAWNET data, the modeled near-surface BC concentrations have a normalized mean bias (NMB) of –53%. Note that anthropogenic BC emissions went up by a factor of 1.18 between 2006–2007 and 2010–2014. An emissions adjusted comparison would result in an even larger underestimation. There are several reasons that might cause low bias in this comparison. Liu et al. (2012) and H. Wang et al. (2013) have previously found underestimation of BC concentrations over China in CAM5 model and suggested the BC emissions may be significantly underestimated. Using the global chemical transport model GEOS-Chem together with emissions in 2006, Fu et al. (2012) found the simulated BC concentrations in China were underestimated by 56%. With HTAP emissions at the year 2010 level, Li et al. (2016) showed a low bias of 37% in simulated BC concentration in China. Large wet removal rate and short lifetime of aerosols, resulting from the too frequent liquid-containing cloud and fast precipitation scavenging in CAM5, also lead to the lower concentrations of BC (Wang et al., 2011; Liu et al., 2012; H. Wang et al., 2013).

Another potential cause for a bias in this comparison is spatial sampling bias. Half of the CAWNET sites are located in urban areas, which will tend to have high values near sources, whereas the modeled values represent averages over large grid cells (R. Wang et al., 2014), as further discussed below.

The model captures well the spatial distribution and seasonal variation of BC concentrations in China, having a statistically significant correlation coefficient of +0.58 between simulated and observed seasonal BC concentrations between modeled and CAWNET values.

3.2 Aerosol absorption optical depth of BC

To evaluate the simulated aerosol absorption optical depth (AAOD) of BC, the AAOD data from AERONET (Holben et al., 2001) are used here. The locations of

Atmos. Chem. Phys. Discuss., doi:10.5194/acp-2016-1032, 2016
Manuscript under review for journal Atmos. Chem. Phys.
Published: 29 November 2016

AERONET sites in China are shown in Figure S1b. The observed AAOD are averaged over years of 2010–2014 over 7 sites and 2005–2010 over 3 sites with data available. Most AERONET sites are over eastern and central China. AAOD of BC at 550nm are calculated by interpolating AAOD at 440 and 675 nm and removing AAOD of dust from the retrieved AERONET AAOD following Bond et al. (2013). Figure 3b compares the observed and simulated seasonal mean AAOD of BC at 550nm and Table S2 summarizes the comparisons in different regions. The model has a low bias in simulating AAOD of BC in China, smaller than the bias in near-surface concentrations, with a NMB of –16% (Figure 3a). As is the case with surface concentrations, this bias could be due to model issues, such as BC transport or optical parameterization; an underestimate in emissions; or spatial sampling bias, although spatial sampling bias is likely to be less important for the BC column than for surface concentrations. Simulated AAOD of BC are within the range of one third to 3 times of observed values at most sites, with the spatial distribution and seasonal variation broadly captured by the model. Note that all but one of the observations are located in the North and South China regions, and simulated BC AAOD are, on average, similar to observations there. The AAOD from one observation site in Central-West China is higher than the modeled value.

Figure 4 shows the spatial distribution of simulated seasonal mean AAOD of total aerosols and Aerosol Index (AI) derived from Ozone Monitoring Instrument (OMI) measurements over years of 2010–2014. AI is a measure of absorbing aerosols including BC and dust. Compared to satellite AI data, the model roughly reproduces spatial distribution of total AAOD in China, with large values over North, South, and Southwest China in all seasons. AI from derived from Total Ozone Mapping Spectrometer (TOMS) measurements also show similar spatial pattern as simulated AAOD (Figure S2). It should be noted that, besides BC, dust particles also largely contribute to AI and produces large AI values over Northwest China.

To examine the potential model bias more broadly we compared the difference of AAOD and AI western China and eastern China (Fig. 4). Averaging AI and AAOD broadly over eastern and western China, we find that AAOD/AI is 0.048 over eastern

Atmos. Chem. Phys. Discuss., doi:10.5194/acp-2016-1032, 2016
Manuscript under review for journal Atmos. Chem. Phys.
Published: 29 November 2016

China and 0.031 over western China. If we assume the simulated AAOD do not have large bias over eastern China compared to observations, then this difference hints at a possible underestimation of BC column burden in the model over the western regions. It is somewhat difficult to draw a firm conclusion, however, given the likely differential role of dust, and model biases modeling dust, and possible biases in satellite derived AI values.

4. Source contributions to BC concentrations, transport and direct radiative forcing

4.1. Source contributions to seasonal mean BC concentrations

Figure 5 shows the simulated spatial distribution of seasonal near-surface BC concentrations originating from the seven tagged source regions in continental China and all other sources from outside China (rest of the world, RW) and Table S3 summarizes these source-receptor relationships. It is not surprising that regional emissions largely influence BC concentrations in the same region. For example, emissions of BC from North China give 5.8 μg m^{-3} of BC concentrations over North China in DJF, whereas they only account for less than 1.3 μg m^{-3} over other regions in China. However, the relatively small amount of BC from upwind source regions can also be a large contributor to receptor regions near the strong sources. BC emissions from North China contribute large amount to concentrations over South, Southwest, Central-West, and Northeast China. BC emissions from South and Southwest China also produce a widespread impact on BC over other neighboring regions. The impacts of BC emitted from the remaining China regions are relatively small both in local and non-local regions due to weak emissions (Fig. 1b). All the sources in China have the largest impact in DJF, resulting from the strong BC emissions in winter, while emissions from outside China have the largest impact on BC over China in MAM due to the seasonal high biomass burning over Southeast Asia and the strong springtime southwesterly winds.

Averaged over continental China, emissions of BC from North China produce mean BC concentrations of 0.4–1.1 μg m^{-3}, followed by 0.2–0.4 μg m^{-3} from South

Atmos. Chem. Phys. Discuss., doi:10.5194/acp-2016-1032, 2016
Manuscript under review for journal Atmos. Chem. Phys.
Published: 29 November 2016

Atmospheric Chemistry and Physics Discussions

China and 0.1–0.2 μg m^{-3} from Southwest China emissions. For emissions over Central-West China, Northeast China, Northwest China, and Tibetan Plateau, their individual impact is less than 0.15 μg m^{-3}. In contrast, emissions from outside China result in 0.13 μg m^{-3} of BC concentrations in China in MAM and less than 0.10 μg m^{-3} in other seasons. The simulated source contributions to column burden of BC are shown in Figure S3. They present a very similar spatial distribution and seasonal variation to those of near-surface BC concentrations. However, the emissions from outside China have a larger impact on the average column burden of BC over China than on surface concentrations, with a magnitude of 0.5 mg m^{-2} in MAM, which is as the same as that from sources in North China.

Figure 6 shows the spatial distribution of simulated relative contributions to near-surface BC concentrations from sources in the seven regions in continental China and those outside China by season. (The same plots for BC column burden are shown in Figure S4.) For regions with higher emissions, their BC concentrations are dominated by local emissions. In contrast, BC levels, especially column burden of BC, over central and western China with lower emissions are strongly influenced by non-local sources. Emissions from outside China can be the largest contributor to BC over these regions. During DJF, MAM and SON, they contribute more than 70% to both surface concentrations and column burden of BC in Tibetan Plateau, which is important to the climate change due to the large climate efficacy of BC in snow (Qian et al., 2011) and acceleration of snowmelt through elevated BC heat pump mechanism (Lau et al., 2010). BC emissions from outside China also account for a quite significant fraction of surface concentrations over Northwest and Southwest China in MAM, which contribute to poor air quality over these regions.

Figure 7 summarizes source attribution for spatially averaged seasonal surface BC concentrations for the seven receptor regions and continental China combined (CN). Over North China, the majority of the BC concentrations are attributed to local emissions in all seasons, with seasonal fractional contributions of 83–93%. Over South China, the seasonal contributions from local emissions are in the range of 64–87%. Emissions from North China account for 30% of BC concentrations over South

Atmos. Chem. Phys. Discuss., doi:10.5194/acp-2016-1032, 2016
Manuscript under review for journal Atmos. Chem. Phys.
Published: 29 November 2016

China in DJF, resulting from the wintertime northwesterly winds (Figure S5a), while emissions from outside China contribute about 10% in MAM due to the strong springtime biomass burning over southeast Asia and southwesterly winds transporting BC from southeast Asia to South China (Figure S5b). Southwest China has a similar level of local influence, with 59–79% of the BC concentration from local emissions, whereas 17% are due to emissions from outside China world transported by westerly winds in MAM.

Non-local emissions from Southwest and North China contribute 27–49% of BC concentration in Central-West China. North China emissions play an important role in BC concentrations over Northeast China, with relative contributions in a range of 22–36% in MAM, JJA and SON, while only 12% in DJF, which is associated with northwesterly winds in winter preventing northward transport of BC from North China to Northeast China. Over Northwest China and Tibetan Plateau, 22–40% and 43–76%, respectively, of BC originate from emissions outside China due to the low emissions over the less economically developed western China. For all of continental China as the receptor, the seasonal BC concentrations are largely attributed to the emissions from North China and South China, with relative contributions ranging from 43–50% and 18–24%, respectively, followed by contributions from Southwest China (10–13%) and outside China (4–12%).

The source region contributions to column burden of BC in each receptor regions in China are shown in Figure S6. In general, impacts on the non-local BC column burden are larger than on surface concentrations because aerosol transport is relatively easier in free-troposphere than in the boundary layer (e.g., Yang et al., 2015). Column burdens of BC averaged over continental China result mainly from emissions in North China and outside China, with relative contributions ranging from 31–42% and 14–31%, respectively.

4.2. Source contributions during polluted days

Knowing the source attribution of BC during polluted days in China is important for policy makers, which could provide an effective way for the mitigation of poor air

Atmos. Chem. Phys. Discuss., doi:10.5194/acp-2016-1032, 2016
Manuscript under review for journal Atmos. Chem. Phys.
Published: 29 November 2016

quality. Here, the polluted days are simply identified as days with daily concentrations of BC higher than 90th percentile of probability density function in each receptor regions. A total of different 45 days in winter in the 5-year simulation are identified as polluted days for each region in China.

Figure 8 shows the DJF composite differences in near-surface BC concentrations and winds at 850 hPa between polluted and normal days for each receptor region, and Figure 9 summarizes the source contributions to the differences. When North China is under the polluted condition, BC concentrations are higher by more than 70% compared to DJF average over North China (Fig. 2a), with a maximum increase exceeding 5 μg m^{-3}. North China local emissions contribute 5.4 μg m^{-3} to the averaged increase in BC concentrations over North China during North China polluted days, about 90% of the total increase. In winter, eastern China is dominated by strong northwesterly winds (Figure S4a). The anomalous southerly winds during polluted days (relative to DJF average) over North China prevent the high BC concentrations from being transported to South China, leading to a reduced ventilation and accumulated aerosols in North China.

Over South China, BC concentrations increase by up to 2 μg m^{-3}, in part due to the transport from North China by anomalous northerly winds in the north of South China in South China polluted days. On average, contribution of North China emissions to mean concentrations over South China increases by 1.2 μg m^{-3} (48% of total increase) during the South China polluted days.

During polluted days in Southwest China, the anomalous northeasterly winds in the east part of Southwest China bring in BC from the highly polluted eastern China, resulting in 1.1 μg m^{-3} increase (53% of total increase) in the Southwest China, which is as similar magnitude as the 1.0 μg m^{-3} contribution from the Southwest China local emissions.

The increase in BC concentrations during polluted days over Central-West China is also largely influenced by the accumulation effect of the anomalous winds over eastern and central China, which also transport BC from Southwest and eastern China into the receptor region.

Atmos. Chem. Phys. Discuss., doi:10.5194/acp-2016-1032, 2016
Manuscript under review for journal Atmos. Chem. Phys.
Published: 29 November 2016

461 The polluted days in Northeast China are caused by both the accumulation of
462 local emissions due to the reduced prevailing northeasterly winds and anomalous
463 transport of BC from North China.
464 Emissions from outside China could contribute to increases in BC concentrations
465 over Northwest China and Tibetan Plateau during polluted days. However, during
466 wintertime regional polluted days in eastern and central China, the contributions of
467 emissions from outside China do not have a significant influence on the changes in
468 BC concentrations.
469 These results suggest that the transport of aerosols plays an important role in
470 increasing BC concentrations during regional polluted days in eastern and central
471 China. Reductions in local emissions could benefit mitigation of both local and
472 non-local haze in China. Emissions from outside China are not as important to hazy
473 pollution in eastern and central China, where haze episodes occur frequently in winter
474 due to relatively high anthropogenic aerosol emissions and abnormal meteorological
475 conditions (Sun et al., 2014; R. H. Zhang et al., 2014; Yang et al., 2016). Note that, in
476 this study, we only focus on the source-receptor relationships related to the wind
477 anomalies during polluted days. In addition to winds, changes in other meteorological
478 fields, such as precipitation, temperature, humidity, and planetary boundary layer
479 height, could also influence the contributions of local aerosols between polluted and
480 normal days. Although the BC emissions used in the simulation include a seasonal
481 variability that could cause some variations in simulated concentrations, the monthly
482 variability in DJF of BC emissions is less than 4% over China, which is negligible
483 compared to the differences in concentrations between polluted and normal days.
484

485 **4.3. Source contributions to trans-boundary and trans-Pacific transport**

486 Considering the large contributions of emissions from Southeast Asia to MAM BC
487 concentrations in the southwest China (Figure 6) and the large outflow of aerosols
488 from East Asia in springtime (Yu et al., 2008), it is valuable to examine the inflow and
489 outflow of BC in China. Figures S7a and S7b show the vertical distribution of source
490 contributions of emissions from outside China to BC concentrations averaged over

Atmos. Chem. Phys. Discuss., doi:10.5194/acp-2016-1032, 2016
Manuscript under review for journal Atmos. Chem. Phys.
Published: 29 November 2016

75°–120°E and 25°–35°N, respectively, around the south boundary of continental China in MAM. High concentrations of BC originating from Southeast Asia are lifted to the free atmosphere in the south slope of Tibetan Plateau. Then westerly winds transport these BC particles to Southwest China and South China in both low- and mid-troposphere. Figures S7c and S7d present the contributions of emissions from China to BC concentrations averaged over 120°–135°E and 20°–50°N, respectively, around the east boundary of continental China. In MAM, the northward meridional winds over 25°–35°N and the southward meridional winds over 40°–50°N lead to the accumulation of BC in the lower atmosphere in eastern China. Westerly winds then transport these BC out of China mostly under 500 hPa.

Figure 10 shows the spatial distribution of column burden and surface concentrations of BC resulting from emissions in and outside China in MAM. Column burden is used to represent the outflow in this study following previous studies (Chin et al., 2007; Hadley et al., 2007). There are strong outflows across the Pacific Ocean originating from emissions both in and outside China. Emissions from China contribute 0.19 mg m^{-2} (or 53%) of MAM mean BC along 150°E averaged over 20°–60°N, whereas emissions outside China contribute 0.17 mg m^{-2} (or 47%). It suggests that both emissions from China and outside China are important for the outflow from East Asia. The yearly contribution from emissions from China in this study is 58%, similar to 61% in Matsui et al. (2013) calculated based on eastward BC mass flux using WRF-CMAQ model with INTEX-B missions. Averaged over western United States (125°–105°W, 30°–50°N), emissions from China account for 7% of near-surface BC concentrations and 25% in column burden in MAM, indicating that emissions from China could have a significant impact on air quality in western United States. More than half of the China contribution to BC over western United States originates from eastern China (i.e., the tagged North and South China).

4.4. Source contributions to direct radiative forcing

The high concentrations of BC in China could also have a significant impact on the climate system through atmospheric heating or direct radiative forcing. As shown

Atmos. Chem. Phys. Discuss., doi:10.5194/acp-2016-1032, 2016
Manuscript under review for journal Atmos. Chem. Phys.
Published: 29 November 2016

in Figure 11, the annual mean direct radiative forcing (DRF) of BC at TOA is as high as 3–4 W m^{-2} at some locations. Similar to the source attributions of BC concentrations (Figure 5) and burden (Figure S3), regional sources contribute the largest to DRF over the respective local regions. Among all the source regions in China, emissions from North, South, and Southwest China contribute the largest to local DRF of BC, with maximum DRF in a range of 3–5, 2–3, and 3–5 W m^{-2}, respectively. Other sources regions in China have relatively low contributions, with maximum values less than 2 W m^{-2}. Emissions outside China lead to 1–2 W m^{-2} of DRF of BC over South, Southwest, Northwest China and Tibetan Plateau, and 0.2–1 W m^{-2} over other parts of China, an effect that is quite widespread.

The total DRF of BC averaged over continental China simulated in this study is 2.27 W m^{-2}, larger than 0.75–1.46 W m^{-2} in previous studies (Wu et al., 2008; Zhuang et al., 2011; Zhuang et al., 2013; Li et al., 2016), probably due to the different emissions in the time periods of study. The total BC emissions averaged over continental China were 1005 Gg C yr^{-1} for years 1993–2003 in Wu et al. (2008), 1811 Gg C yr^{-1} for year 2006 in Zhuang et al. (2011, 2013), and 1840 Gg C yr^{-1} for year 2010 in Li et al. (2016), whereas 2497 Gg C yr^{-1} for year 2010–2014 used in this study. Emissions outside China have the largest contributions to DRF of BC in China compared to any of the individual source regions in China, with an averaged contribution of 0.77 W m^{-2} (34%). This fractional contribution from emissions outside China is larger than 25% in Li et al. (2016), however we use different emissions, model and meteorology. Emissions from North China result in 0.56 W m^{-2} (25%) of DRF of BC over China, followed by 0.33 W m^{-2} (15%) and 0.31 W m^{-2} (14%) from South China and Southwest China, respectively. Emissions from Central-West, Northeast, Northwest China, and Tibetan Plateau taken together account for 0.30 W m^{-2} (13%) of DRF of BC over China.

Figure 12a shows the seasonal mean DRF of BC averaged over China as a function of regional BC emissions. Because of high emissions, DRF of BC emitted from North China is the largest in all seasons, with values in a range of 0.5–0.7 W m^{-2} averaged over China, followed by 0.2–0.5 W m^{-2} from South and Southwest China.

Atmos. Chem. Phys. Discuss., doi:10.5194/acp-2016-1032, 2016
Manuscript under review for journal Atmos. Chem. Phys.
Published: 29 November 2016

Atmospheric Chemistry and Physics Discussions

551 BC from the other tagged regions in China contribute less than 0.2 W m^{-2} in all
552 seasons. In general, BC DRF in each season is proportional to its emission rate.
553 Figure 12b presents the seasonal DRF efficiency of BC emitted from the tagged
554 regions and Table S4 summarizes these efficiencies. The variability of DRF efficiency
555 for forcing over China is determined by several factors, such as incoming solar
556 radiation (location of source regions), BC column burden and vertical distribution, and
557 transport out of the region. The China DRF efficiency is largest in western China (NW
558 and TP). This spatial pattern was also found by Henze et al. (2012). It can be
559 explained by the increase of multiple scattering effects and attenuation of the
560 transmitted radiation for large AOD (García et al., 2012). The Northeast China region
561 has a low China DRF efficiency due to transport eastward outside of China. The
562 remaining central and southern China regions have China DRF efficiencies that are
563 fairly consistent, varying by 20-30% about the average.
564 DRF efficiencies of BC from most regions have higher values in JJA and lower
565 values in DJF. This is primarily due to more incoming solar radiation in summer.
566 Insolation is the largest over Northwest China in JJA, together with less precipitation
567 than other regions, resulting in large DRF efficiency there. Global BC DRF efficiency,
568 particularly the annual average, is fairly similar for central, southern, and eastern
569 China regions (Fig. 12c, d). Global efficiency is still much higher for the western
570 regions.
571 BC emission reductions may impact mitigation of climate change and improve air
572 quality. To compare the relative importance of climate and air quality effects of BC
573 from different regions in China, Fig. 13 shows the near-surface concentration and
574 column burden efficiency of BC over China and globally and Table S5 summarizes
575 these efficiencies. For near-surface concentration (Fig. 13a and 13b), the efficiencies
576 are largest in DJF and lowest in JJA, in contrast to the DRF efficiencies, resulting
577 from the less precipitation and wet deposition of aerosols in winter. Unlike the DRF
578 efficiencies, the near-surface concentration efficiencies over eastern China are
579 similar and even larger than those for central and western China. These results

Atmos. Chem. Phys. Discuss., doi:10.5194/acp-2016-1032, 2016
Manuscript under review for journal Atmos. Chem. Phys.
Published: 29 November 2016

suggest that reduction in BC emissions in eastern China could benefit more on the regional air quality in China, especially in winter haze season.

The relative distributions of column burden efficiencies (Fig. 13c and 13d) are similar to the DRF efficiencies for the major emitting region in China, indicating that aerosol lifetime in atmosphere drives DRF that influences regional and global climate. The western regions (NW and TP), as expected, have a higher forcing per unit column burden.

5. Conclusions

In this study, the Community Earth System Model (CESM) with a source-tagging technique is used to quantify the contributions of BC emitted from seven regions in continental China, including North China (NC), South China (SC), Southwest China (SW), Central-West China (CW), Northeast China (NE), Northwest China (NW), and Tibetan Plateau (TP), and sources outside China (RW) to concentrations, haze formation, trans-boundary and trans-Pacific transport, and direct radiative forcing (DRF) of BC in China. The anthropogenic emissions of BC for years 2009-2014 used in this study were developed for the Coupled Model Intercomparison Project Phase 6 (CMIP6) from the Community Emissions Data System (CEDS). The annual total emission of BC from continental China is 2497 Gg C averaged over years 2010–2014. The model captures well the spatial distribution and seasonal variation in China. AAOD compares well with measurements, which are largely located in central and eastern China. Surface BC concentrations are underestimated by 53% compared to point observations.

The individual source regions are the largest contributors to their local BC concentration levels. Over North China where the air quality is often poor, about 90% of near-surface BC concentration is contributed by local emissions. However, some source regions also impact BC in neighboring regions. Due to the seasonal variability of winds and emission rates, emissions from North China account for 30% of near-surface BC concentrations over South China in DJF

Atmos. Chem. Phys. Discuss., doi:10.5194/acp-2016-1032, 2016
Manuscript under review for journal Atmos. Chem. Phys.
Published: 29 November 2016

(December-January-February), while emissions from outside China contribute about 10% in MAM (March-April-May). Over Southwest China, 17% of BC in MAM comes from sources outside China. Southwest and North China emissions contribute largely to BC in Central-West China. North China emissions have a contribution in a range of 12–36% to BC concentrations in Northeast China. Over Northwest China and Tibetan Plateau, more than 20% and 40% of BC, respectively, originates from emissions outside China. These indicate that, for regions with high emissions, their BC concentrations are dominated by local emissions. In contrast, BC levels over central and western China with lower emissions are more strongly influenced by non-local emissions. For all continental China as a whole, seasonal BC concentrations are largely due to emissions from North and South China, with relative contributions ranging from 43–50% and 18–24%, respectively, followed by contributions from Southwest (10–13%) and outside China (4–12%).

Emissions from non-local sources together with abnormal winds are one of the important factors contributing to high winter time pollution events in China. Over South China, about 50% of the increase in BC concentrations during high pollution conditions results from North China emissions. The increases in BC concentrations during polluted days over Southwest, Central-West and Northeast China are strongly influenced by emissions from eastern China. Emissions from outside China could contribute significantly to increases in BC concentrations over Northwest China and Tibetan Plateau during their polluted days. However, emissions from outside China do not have a significant contribution to haze in eastern and central China, suggesting that reduction in emissions within China would be needed to mitigate both local and non-local BC concentrations under high-polluted conditions.

Emissions from regions in and outside China both account for about half of BC outflow from East Asia, suggesting that emissions from China and other regions are equally important for the BC outflow from East Asia. Through long-range transport, emissions from China result in 7% of near-surface BC concentration and 25% in column burden over western United States in MAM, indicating that emissions from China are could have an impact on air quality in western United States.

Atmos. Chem. Phys. Discuss., doi:10.5194/acp-2016-1032, 2016
Manuscript under review for journal Atmos. Chem. Phys.
Published: 29 November 2016

640 The total DRF of BC averaged over continental China simulated in this study is
641 2.27 W m^{-2}. Among the tagged regions, emissions outside China have the largest
642 single contribution to DRF of BC in China, with an average contribution of 34%,
643 followed by 25%, 15%, and 14% due to emissions from North, South and Southwest
644 China, respectively. DRF efficiencies over eastern China are small compared to
645 central and western China in all seasons. It can be explained by the increase of
646 multiple scattering effects and attenuation of the transmitted radiation for large AOD.
647 For near-surface concentration, the efficiencies are largest in DJF and lowest in JJA,
648 and efficiencies over eastern China are similar and even larger than central and
649 western China. These suggest that reduction in BC emissions over eastern China
650 could benefit more on the regional air quality in China, especially in winter haze
651 season.
652 Note that the model largely underestimates BC concentrations over China,
653 compared to the observation, which has also been reported in many previous studies
654 using different models and different emission inventories (e.g., Liu et al., 2012; Fu et
655 al., 2012; H. Wang et al., 2013; R. Wang et al., 2014; Li et al., 2016). One possible
656 reason is that in situ measurements are point observations, while the model does not
657 treat the subgrid variability of aerosols and assumes aerosols are uniformly
658 distributed over the grid cell. R. Wang et al. (2014) found a reduction of negative bias
659 (from −88% to −35%) in the modeled surface BC concentrations when using
660 high-resolution emissions and modeling at 0.5° X 0.7° resolution. They find, however,
661 that modeling over the North China Plain at an even higher resolution of 0.1°, further
662 reduced the surface concentration bias there from 29% to 8%. This result indicates
663 that the siting of observational stations can result in an artificial bias when comparing
664 with relatively coarse model results. Further investigation of this siting/resolution bias
665 is warranted, including investigation if this type of bias might extend, presumably to a
666 lesser exent, also to AAOD measurements.
667 Further reasons that could contribute to this bias are emission underestimation or
668 inaccurate aerosol processes in the model. Given that the differences between
669 modeled observed AAOD over eastern China are relatively small (–18%), we

Atmos. Chem. Phys. Discuss., doi:10.5194/acp-2016-1032, 2016
Manuscript under review for journal Atmos. Chem. Phys.
Published: 29 November 2016

conclude that, given current evidence, the total amount of atmospheric BC in these simulations is reasonable at least in this sub-region.

Over eastern China, the BC concentrations are dominated by local emissions in this study, with local contribution of 64–93%. The underestimation of simulated BC concentrations over eastern China is more likely due to either underestimation of local emissions, too much aerosol removal within these regions, or resolution bias between observations and model grids. Over western China, 22–76% of the BC originates from emissions outside China. Thus biases of simulated BC concentrations could also come from underestimation of emissions outside China and or too much removal of BC during long-range transport. Satellite data are a promising method to validate modeling and emissions inventories, given that they do not depend on the location of observing stations, providing more uniform spatial coverage. A comparison of modeled AAOD and satellite aerosol index (AI) provides an indication that the modeled burden in western China is underestimated, although the role of dust needs to be better characterized.

Acknowledgments.
This research was supported by the National Atmospheric and Space Administration's Atmospheric Composition: Modeling and Analysis Program (ACMAP), award NNH15AZ64I. We also acknowledge additional support from the U.S. Department of Energy (DOE), Office of Science, Biological and Environmental Research. The Pacific Northwest National Laboratory is operated for DOE by Battelle Memorial Institute under contract DE-AC05-76RLO1830. The CESM project was supported by the National Science Foundation and the DOE Office of Science. The satellite-derived Total Ozone Mapping Spectromenter Aerosol Index monthly data sets are obtained from the Web site at http://disc.sci.gsfc.nasa.gov/data-holdings/PIP/aerosol_index.shtml. The National Energy Research Scientific Computing Center (NERSC) provided computational resources. Model results are available through NERSC upon request.

Atmos. Chem. Phys. Discuss., doi:10.5194/acp-2016-1032, 2016
Manuscript under review for journal Atmos. Chem. Phys.
Published: 29 November 2016

Atmospheric Chemistry and Physics Discussions

700 **References**

701

702 Anenberg, S. C., K. Talgo, S. Arunachalam, P. Dolwick, C. Jang, and J. J. West
703 (2011), Impacts of global, regional, and sectoral black carbon emission
704 reductions on surface air quality and human mortality, Atmos. Chem. Phys., 11,
705 7253-7267, doi:10.5194/acp-11-7253-2011.

706

707 Bond, T. C., D. G. Streets, K. F. Yarber, S. M. Nelson, J.-H. Woo, and Z. Klimont
708 (2004), A technology-based global inventory of black and organic carbon
709 emissions from combustion, J. Geophys. Res., 109, D14203,
710 doi:10.1029/2003JD003697.

711

712 Bond, T. C., E. Bhardwaj, R. Dong, R. Jogani, S. Jung, C. Roden, D. G. Streets, and
713 N. M. Trautmann (2007), Historical emissions of black and organic carbon
714 aerosol from energy-related combustion, 1850–2000, Global Biogeochem.
715 Cycles, 21, GB2018, doi:10.1029/2006GB002840.

716

717 Bond, T. C., et al. (2013), Bounding the role of black carbon in the climate system: A
718 scientific assessment, J. Geophys. Res. Atmos., 118, 5380–5552,
719 doi:10.1002/jgrd.50171.

720

721 Chin, M., T. Diehl, P. Ginoux, and W. Malm (2007), Intercontinental transport of
722 pollution and dust aerosols: implications for regional air quality, Atmos. Chem.
723 Phys., 7, 5501-5517, doi:10.5194/acp-7-5501-2007.
724
725 Ding, Y. H., and Y. J. Liu (2014), Analysis of long-term variations of fog and haze in
726 China in recent 50 years and their relations with atmospheric humidity, Sci. China
727 Earth Sci., 57, 36–46, doi:10.1007/s11430-013-4792-1.
728
729 Flanner, M. G., C. S. Zender, J. T. Randerson, and P. J. Rasch (2007), Present day
730 climate forcing and response from black carbon in snow, J. Geophys. Res., 112,
731 D11202, doi:10.1029/2006JD008003.
732
733 Fu, T.-M., J. J. Cao, X. Y. Zhang, S. C. Lee, Q. Zhang, Y. M. Han, W. J. Qu, Z. Han,
734 R. Zhang, Y. X. Wang, D. Chen, and D. K. Henze (2012), Carbonaceous aerosols
735 in China: top-down constraints on primary sources and estimation of secondary
736 contribution, Atmos. Chem. Phys., 12, 2725-2746,
737 doi:10.5194/acp-12-2725-2012.
738
739 García, O. E., J. P. Díaz, F. J. Expósito, A. M. Díaz, O. Dubovik, Y. Derimian, P.
740 Dubuisson, and J.-C. Roger (2012), Shortwave radiative forcing and efficiency of
741 key aerosol types using AERONET data, Atmos. Chem. Phys., 12, 5129-5145,
742 doi:10.5194/acp-12-5129-2012.

743

744 Ghan, S. J., and R. A. Zaveri (2007), Parameterization of optical properties for
745 hydrated internally mixed aerosol, J. Geophys. Res., 112, D10201,
746 doi:10.1029/2006JD007927.

747

748 Ghan, S. J. (2013), Technical Note: Estimating aerosol effects on cloud radiative
749 forcing, Atmos. Chem. Phys., 13, 9971-9974, doi:10.5194/acp-13-9971-2013.

750

751 Hadley, O. L., V. Ramanathan, G. R. Carmichael, Y. Tang, C. E. Corrigan, G. C.
752 Roberts, and G. S. Mauger (2007), Trans-Pacific transport of black carbon and
753 fine aerosols (D < 2.5 μm) into North America, J. Geophys. Res., 112, D05309,
754 doi:10.1029/2006JD007632.

755

756 Henze, D. K., D. T. Shindell, F. Akhtar, R. J. D. Spurr, R. W. Pinder, D. Loughlin, M.
757 Kopacz, K. Singh, and C. Shim (2012), Spatially refined aerosol direct radiative
758 forcing efficiencies, Environ. Sci. Technol., 46, 9511–9518,
759 doi:10.1021/es301993s.

760

761 Holben, B. N., et al. (2001), An emerging ground-based aerosol climatology: Aerosol
762 optical depth from AERONET, J. Geophys. Res., 106(D11), 12067–12097,
763 doi:10.1029/2001JD900014.

764

765 Hurrell, J. W., et al. (2013), The Community Earth System Model: A Framework for
766 Collaborative Research, B. Am. Meteorol. Soc., 94, 1339–1360,
767 doi:10.1175/BAMS-D-12-00121.
768
769 IPCC, 2013, Climate Change 2013: the Physical Science Basis. Contribution of
770 Working Group I to the Fifth Assessment Report of the Intergovernmental Panel
771 on Climate Change. Cambridge University Press, Cambridge, United Kingdom
772 and New York, NY, USA, p. 1535.
773
774 Jacobson, M. Z. (2006), Effects of externally-through-internally-mixed soot inclusions
775 within clouds and precipitation on global climate, J. Phys. Chem. A, 110, 6860–
776 6873, doi:10.1021/Jp056391r.
777
778 Janssen, N. A. H., M. E. Gerlofs-Nijiland, T. Lanki, R. O. Salonen, F. Cassee, G.
779 Hoek, P. Fischer, B. Brunekreef, and M. Krzyzanowski (2012), Health Effects of
780 Black Carbon, World Health Organization, Copenhagen.
781
782 Janssens-Maenhout, G., et al. (2015), HTAP_v2.2: a mosaic of regional and global
783 emission grid maps for 2008 and 2010 to study hemispheric transport of air
784 pollution, Atmos. Chem. Phys., 15, 11411-11432,
785 doi:10.5194/acp-15-11411-2015.
786

787 Jiao, C., et al. (2014), An AeroCom assessment of black carbon in Arctic snow and
788 sea ice, Atmos. Chem. Phys., 14, 2399–2417, doi:10.5194/acp-14-2399-2014.
789
790 Lau, K.-M., M. K. Kim, K.-M. Kim, and W. S. Lee (2010), Enhanced surface warming
791 and accelerated snow melt in the Himalayas and Tibetan Plateau induced by
792 absorbing aerosols, Environ. Res. Lett., 5, 025204,
793 doi:10.1088/1748-9326/5/2/025204.
794
795 Li, K., H. Liao, Y. H. Mao, and D. A. Ridley (2016), Source sector and region
796 contributions to concentration and direct radiative forcing of black carbon in
797 China, Atmos. Environ., 124, 351–366, doi:10.1016/j.atmosenv.2015.06.014.
798
799 Liao, H., W. Y. Chang, and Y. Yang (2015), Climatic effects of air pollutants over
800 China: A review, Adv. Atmos. Sci., 32, 115–139, doi:10.1007/s00376-014-0013-x.
801
802 Liu, X., et al. (2012), Toward a minimal representation of aerosols in climate models:
803 Description and evaluation in the Community Atmosphere Model CAM5, Geosci.
804 Model Dev., 5, 709–739, doi:10.5194/gmd-5-709-2012.
805
806 Lou, S., L. M. Russell, Y. Yang, L. Xu, M. A. Lamjiri, M. J. DeFlorio, A. J. Miller, S. J.
807 Ghan, Y. Liu, and B. Singh (2016), Impacts of the East Asian Monsoon on

springtime dust concentrations over China, J. Geophys. Res. Atmos., 121, 8137–8152, doi:10.1002/2016JD024758.

Ma, P.-L., J. R. Gattiker, X. Liu, and P. J. Rasch (2013a), A novel approach for determining source-receptor relationships in model simulations: a case study of black carbon transport in northern hemisphere winter, Environ. Res. Lett., 8(2), 024042, doi:10.1088/1748-9326/8/2/024042.

Ma, P.-L., P. J. Rasch, H. Wang, K. Zhang, R. C. Easter, S. Tilmes, J. D. Fast, X. Liu, J.-H. Yoon, and J.-F. Lamarque (2013b), The role of circulation features on black carbon transport into the Arctic in the Community Atmosphere Model version 5 (CAM5), J. Geophys. Res. Atmos., 118, 4657–4669, doi:10.1002/jgrd.50411.

Matsui, H., M. Koike, Y. Kondo, N. Oshima, N. Moteki, Y. Kanaya, A. Takami, and M. Irwin (2013), Seasonal variations of Asian black carbon outflow to the Pacific: Contribution from anthropogenic sources in China and biomass burning sources in Siberia and Southeast Asia, J. Geophys. Res. Atmos., 118, 9948–9967, doi:10.1002/jgrd.50702.

McFarquhar, G., and H. Wang (2006), Effects of aerosols on trade wind cumuli over the Indian Ocean: Model simulations, Q. J. R. Meteorol. Soc., 132, 821–843, doi:10.1256/qj.04.179.

Qian, Y., M. G. Flanner, L. R. Leung, and W. Wang (2011), Sensitivity studies on the impacts of Tibetan Plateau snowpack pollution on the Asian hydrological cycle and monsoon climate, Atmos. Chem. Phys., 11, 1929–1948, doi:10.5194/acp-11-1929- 2011.

Qian, Y., H. Wang, R. Zhang, M. G. Flanner, and P. J. Rasch (2014), A sensitivity study on modeling black carbon in snow and its radiative forcing over the Arctic and Northern China, Environ. Res. Lett., 9, 064001, doi:10.1088/1748-9326/9/6/064001.

Qian, Y., T. J. Yasunari, S. J. Doherty, M. G. Flanner, W. K. M. Lau, J. Ming, H. Wang, M. Wang, S. G. Warren, and R. Zhang (2015), Light-absorbing particles in snow and ice: Measurement and modeling of climatic and hydrological impact, *Adv. Atmos. Sci.*, 32(1), 64–91, doi:10.1007/s00376-014-0010-0.

Ramanathan, V., and G. Carmichael (2008), Global and regional climate changes due to black carbon, Nat. Geosci., 1, 221-227, doi:10.1038/ngeo156.

850 Rienecker, M. M., et al. (2011), MERRA: NASA's Modern-Era Retrospective Analysis
851 for Research and Applications, J. Clim., 24(14), 3624–3648,
852 doi:10.1175/JCLI-D-11-00015.1.
853
854 Shindell, D., et al. (2012), Simultaneously mitigating near-term climate change and
855 improving human health and food security, Science, 335(6065), 183-189,
856 doi:10.1126/science.1210026.
857
858 Smith, S. J., and A. Mizrahi (2013), Near-term climate mitigation by short-lived
859 forcers, Proc. Natl. Acad. Sci, 110(35), 14202-14206,
860 doi:10.1073/pnas.1308470110.
861
862 Sun, Y., Q. Jiang, Z. Wang, P. Fu, J. Li, T. Yang, and Y. Yin (2014), Investigation of
863 the sources and evolution processes of severe haze pollution in Beijing in
864 January 2013, J. Geophys. Res. Atmos., 119, 4380–4398,
865 doi:10.1002/2014JD021641.
866
867 Wang, H., R. C. Easter, P. J. Rasch, M. Wang, X. Liu, S. J. Ghan, Y. Qian, J.-H.
868 Yoon, P.-L. Ma, and V. Vinoj (2013), Sensitivity of remote aerosol distributions to
869 representation of cloud-aerosol interactions in a global climate model, Geosci.
870 Model Dev., 6, 765–782, doi:10.5194/gmd-6-765-2013.
871

872 Wang, H., P. J. Rasch, R. C. Easter, B. Singh, R. Zhang, P.-L. Ma, Y. Qian, S. J.
873 Ghan, and N. Beagley (2014), Using an explicit emission tagging method in
874 global modeling of source-receptor relationships for black carbon in the Arctic:
875 Variations, sources, and transport pathways, J. Geophys. Res. Atmos., 119,
876 12,888–12,909, doi:10.1002/ 2014JD022297.
877
878 Wang, L. T., Z. Wei, J. Yang, Y. Zhang, F. F. Zhang, J. Su, C. C. Meng, and Q. Zhang
879 (2014), The 2013 severe haze over southern Hebei, China: model evaluation,
880 source apportionment, and policy implications, Atmos. Chem. Phys., 14, 3151–
881 3173, doi:10.5194/acp-14-3151-2014.
882
883 Wang, M., S. Ghan, M. Ovchinnikov, X. Liu, R. Easter, E. Kassianov, Y. Qian, and H.
884 Morrison (2011), Aerosol indirect effects in a multi-scale aerosol-climate model
885 PNNL-MMF, Atmos. Chem. Phys., 11, 5431–5455,
886 doi:10.5194/acp-11-5431-2011.
887
888 Wang, R., et al. (2014), Exposure to ambient black carbon derived from a unique
889 inventory and high-resolution model, Proc. Natl. Acad. Sci. U. S. A., 111(7),
890 2459–2463, doi:10.1073/pnas.1318763111.
891
892 Wang, X., Y. Wang, J. Hao, Y. Kondo, M. Irwin, J. W. Munger, and Y. Zhao (2013),
893 Top-down estimate of China's black carbon emissions using surface

observations: Sensitivity to observation representativeness and transport model error, J. Geophys. Res. Atmos., 118, 5781–5795, doi:10.1002/jgrd.50397.

Wu, J., C. Fu, Y. Xu, J. P. Tang, W. Wang, and Z. Wang (2008), Simulation of direct effects of black carbon aerosol on temperature and hydrological cycle in Asia by a Regional Climate Model, Meteorol. Atmos. Phys., 100(1), 179–193, doi:10.1007/s00703-008-0302-y.

Yang Y., H. Liao, and S. Lou (2015), Decadal trend and interannual variation of outflow of aerosols from East Asia: Roles of variations in meteorological parameters and emissions, Atmos. Environ., 100, 141-153, doi:10.1016/j.atmosenv.2014.11.004

Yang, Y., H. Liao, and S. Lou (2016), Increase in winter haze over eastern China in recent decades: Roles of variations in meteorological parameters and anthropogenic emissions, J. Geophys. Res. Atmos., 121, doi:10.1002/2016JD025136.

Yu, H., L. A. Remer, M. Chin, H. Bian, R. G. Kleidman, and T. Diehl (2008), A satellite-based assessment of transpacific transport of pollution aerosol, J. Geophys. Res., 113, D14S12, doi:10.1029/2007JD009349.

916 Zhang, K., H. Wan, X. Liu, S. J. Ghan, G. J. Kooperman, P.-L. Ma, P. J. Rasch, D.
917 Neubauer, and U. Lohmann (2014), Technical note: On the use of nudging for
918 aerosol-climate model intercomparison studies, Atmos. Chem. Phys., 14,
919 8631-8645, doi:10.5194/acp-14-8631-2014.
920
921 Zhang, Q., D. G. Streets, G. R. Carmichael, K. B. He, H. Huo, A. Kannari, Z. Klimont,
922 I. S. Park, S. Reddy, J. S. Fu, D. Chen, L. Duan, Y. Lei, L. T. Wang, and Z. L. Yao
923 (2009), Asian emissions in 2006 for the NASA INTEX-B mission, Atmos. Chem.
924 Phys., 9, 5131-5153, doi:10.5194/acp-9-5131-2009.
925
926 Zhang, R. H., Q. Li, and R. N. Zhang (2014), Meteorological conditions for the
927 persistent severe fog and haze event over eastern China in January 2013, Sci.
928 China Earth Sci., 57(1), 26–35, doi:10.1007/s11430-013-4774-3.
929
930 Zhang, R., H. Wang, D. A. Hegg, Y. Qian, S. J. Doherty, C. Dang, P.-L. Ma, P. J.
931 Rasch, and Q. Fu (2015), Quantifying sources of black carbon in western North
932 America using observationally based analysis and an emission tagging technique
933 in the Community Atmosphere Model, Atmos. Chem. Phys., 15, 12805-12822,
934 doi:10.5194/acp-15-12805-2015.
935
936 Zhang, R., H. Wang, Y. Qian, P. J. Rasch, R. C. Easter, P.-L. Ma, B. Singh, J. Huang,
937 and Q. Fu (2015), Quantifying sources, transport, deposition, and radiative

forcing of black carbon over the Himalayas and Tibetan Plateau, Atmos. Chem. Phys., 15, 6205-6223, doi:10.5194/acp-15-6205-2015.

Zhang, X. Y., Y. Q. Wang, X. C. Zhang, W. Guo, and S. L. Gong (2008), Carbonaceous aerosol composition over various regions of China during 2006, J. Geophys. Res., 113, D14111, doi:10.1029/2007JD009525.

Zhang, X. Y., Y. Q. Wang, T. Niu, X. C. Zhang, S. L. Gong, Y. M. Zhang, and J. Y. Sun (2012), Atmospheric aerosol compositions in China: Spatial/temporal variability, chemical signature, regional haze distribution and comparisons with global aerosols, Atmos. Chem. Phys., 12, 779–799, doi:10.5194/acp-12-779-2012.

Zhang, Y. L., et al. (2015), Fossil vs. non-fossil sources of fine carbonaceous aerosols in four Chinese cities during the extreme winter haze episode in 2013, Atmos. Chem. Phys., 15, 1299-1312, doi:10.5194/acp-15-1299-2015.

Zhuang, B. L., F. Jiang, T. J. Wang, S. Li, and B. Zhu (2011), Investigation on the direct radiative effect of fossil fuel black-carbon aerosol over China, Theor. Appl. Climatol., 104(3), 301–312, doi:10.1007/s00704-010-0341-4.

959 Zhuang, B. L., Q. Liu, T. J. Wang, C. Q. Yin, S. Li, M. Xie, F. Jiang, and H. T. Mao
960 (2013), Investigation on semi-direct and indirect climate effects of fossil fuel black
961 carbon aerosol over China, Theor. Appl. Climatol., 114 (3), 651–672,
962 doi:10.1007/s00704-013-0862-8.
963
964 Zhuang, B. L., T. J. Wang, J. Liu, S. Li, M. Xie, X. Q. Yang, C. B. Fu, J. N. Sun, C. Q.
965 Yin, J. B. Liao, J. L. Zhu, and Y. Zhang (2014), Continuous measurement of black
966 carbon aerosol in urban Nanjing of Yangtze River Delta, China, Atmos. Environ.,
967 89, 415–424, doi:10.1016/j.atmosenv.2014.02.052.
968
969
970
971

Atmos. Chem. Phys. Discuss., doi:10.5194/acp-2016-1032, 2016
Manuscript under review for journal Atmos. Chem. Phys.
Published: 29 November 2016

Atmospheric Chemistry and Physics Discussions

Figure Captions

Figure 1. (a) Spatial distribution of annual mean total emissions (anthropogenic plus biomass burning, units: g C m^{-2} yr^{-1}) of black carbon (BC) averaged over 2010–2014. The geographical BC source regions are selected as North China (NC, 109°E–east boundary, 30°–41°N), South China (SC, 109°E–east boundary, south boundary–30°N), Southwest China (SW, 100°–109°N, south boundary–32°N), Central-West China (CW, 100°–109°N, 32°N–north boundary), Northeast China (NE, 109°E–east boundary, 41°N–north boundary), Northwest China (NW, west boundary–100°E, 36°N–north boundary), and Tibetan Plateau (TP, west boundary–100°E, south boundary–36°N) in China and regions outside of China (RW, rest of the world). (b) Seasonal mean total emissions (units: Gg C, Gg = 10^9g) of BC from the seven BC source regions in China.

Figure 2. Simulated seasonal mean near-surface concentrations (left, units: μg m^{-3}) and column burden (right, units: mg m^{-2}) of BC in December-January-February (DJF), March-April-May (MAM), June-July-August (JJA), and September-October-November (SON).

Figure 3. Comparisons of observed and modeled seasonal mean (a) near-surface concentrations (units: μg m^{-3}) and (b) aerosol absorption optical depth (AAOD) of BC in China. Solid lines mark the 1:1 ratios and dashed lines mark the 1:3 and 3:1 ratios. Observed BC concentrations were taken between 2006 and 2007 at 14 sites of the China Meteorological Administration (CMA) Atmosphere Watch Network (CAWNET) (Zhang et al., 2012). Observed AAOD of BC are obtained by removing dust AAOD from total AAOD at 10 sites of the Aerosol Robotic Network (AERONET) (Holben et al., 2001), following Bond et al. (2013). The observed AAOD are averaged over years of 2005–2014 with data available. Correlation coefficient (R) and normalized mean bias (NMB) between observation and simulation are shown on top left of each panel.

Atmos. Chem. Phys. Discuss., doi:10.5194/acp-2016-1032, 2016
Manuscript under review for journal Atmos. Chem. Phys.
Published: 29 November 2016

NMB = 100%× $\sum(M_i - O_i) / \sum O_i$, where M_i and O_i are the modeled and observed values at site i, respectively. Site locations are shown in Figure S1a.

Figure 4. Spatial distribution of seasonal mean AAOD of total aerosols (left) and Aerosol Index (AI) derived from Ozone Monitoring Instrument (OMI) measurements over years of 2010–2014 (right).

Figure 5. Spatial distribution of seasonal mean near-surface concentrations of BC (μg m^{-3}) originating from the seven source regions in China (NC, SC, SW, CW, NE, NW, and TP), marked with black outlines, and sources outside China (RW). Regionally averaged BC in China contributed by individual source regions is shown at the bottom right of each panel.

Figure 6. Spatial distribution of relative contributions (%) to seasonal mean near-surface BC concentrations from each of the tagged source regions.

Figure 7. Relative contributions (%) from the tagged source regions (denoted by colors) to regional mean surface concentrations of BC over seven receptor regions in China (NC, SC, SW, CW, NE, NW, and TP) and China (seven regions combined, CN) in different seasons. The receptor regions are marked on the horizontal axis in each panel.

Figure 8. Composite differences in winds at 850 hPa (m s^{-1}) and near-surface BC concentrations (μg m^{-3}) between polluted and normal days in DJF.

Figure 9. Composite differences in surface BC concentrations (μg m^{-3}) averaged over receptor regions (marked on the horizontal axis) over eastern and central China between polluted and normal days in DJF originating from individual sources regions (bars in each column).

Atmos. Chem. Phys. Discuss., doi:10.5194/acp-2016-1032, 2016
Manuscript under review for journal Atmos. Chem. Phys.
Published: 29 November 2016

1031 **Figure 10.** Spatial distribution of (a, b) column burden (mg m^{-2}) and (c, d)
1032 near-surface concentrations (μg m^{-3}) of BC originating from total emissions inside
1033 (CN) and outside China (RW), respectively, in March-April-May (MAM). The black
1034 solid lines over western (150°E, 20°–60°N) Pacific in panel (a) mark the
1035 cross-sections used to quantify outflow of BC from East Asia. The box over western
1036 United States (125°–105°W, 30°–50°N) in panel (c) is used to quantify BC
1037 concentrations attributed to sources from China.
1038
1039 **Figure 11.** Spatial distribution of annual mean direct radiative forcing of BC (W m^{-2}) at
1040 the top of the atmosphere originating from the tagged BC source regions in China
1041 (NC, SC, SW, CW, NE, NW, and TP) and source outside China (RW). Regionally
1042 averaged forcing in China contributed by individual source regions is shown at the
1043 bottom right of each panel.
1044
1045 **Figure 12.** (a, c) BC seasonal DRF averaged over China as a function of BC
1046 emission fraction (the ratio of regional emission to the total emission over China and
1047 global, respectively, unit: %) for each of the tagged regions. (b, d) Seasonal DRF
1048 efficiency of BC (W m^{-2} Tg^{-1}) for each of the tagged source regions over China and
1049 globally, respectively. The efficiency is defined as the DRF divided by the
1050 corresponding scaled annual emission (seasonal emission multiplied by 4). Error bars
1051 indicate 1-σ of mean values during years 2010–2014.
1052
1053 **Figure 13.** Seasonal (a, b) near-surface concentration (μg m^{-3} Tg^{-1}) and (c, d) column
1054 burden (mg m^{-2} Tg^{-1}) efficiency of BC for each of the tagged source regions over
1055 China and globally, respectively.
1056
1057

Atmos. Chem. Phys. Discuss., doi:10.5194/acp-2016-1032, 2016
Manuscript under review for journal Atmos. Chem. Phys.
Published: 29 November 2016

Atmospheric Chemistry and Physics Discussions

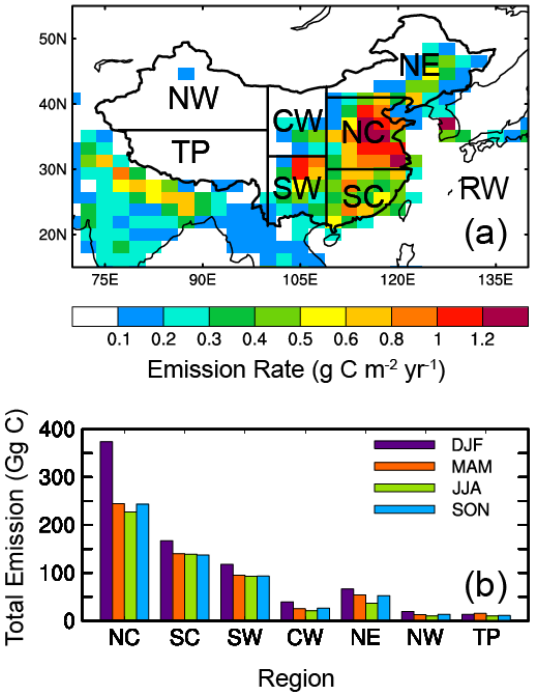

Figure 1. (a) Spatial distribution of annual mean total emissions (anthropogenic plus biomass burning, units: g C m^{-2} yr^{-1}) of black carbon (BC) averaged over 2010–2014. The geographical BC source regions are selected as North China (NC, 109°E–east boundary, 30°–41°N), South China (SC, 109°E–east boundary, south boundary–30°N), Southwest China (SW, 100°–109°N, south boundary–32°N), Central-West China (CW, 100°–109°N, 32°N–north boundary), Northeast China (NE, 109°E–east boundary, 41°N–north boundary), Northwest China (NW, west boundary–100°E, 36°N–north boundary), and Tibetan Plateau (TP, west boundary–100°E, south boundary–36°N) in China and regions outside of China (RW, rest of the world). (b) Seasonal mean total emissions (units: Gg C, Gg = 10^9g) of BC from the seven BC source regions in China.

Atmos. Chem. Phys. Discuss., doi:10.5194/acp-2016-1032, 2016
Manuscript under review for journal Atmos. Chem. Phys.
Published: 29 November 2016

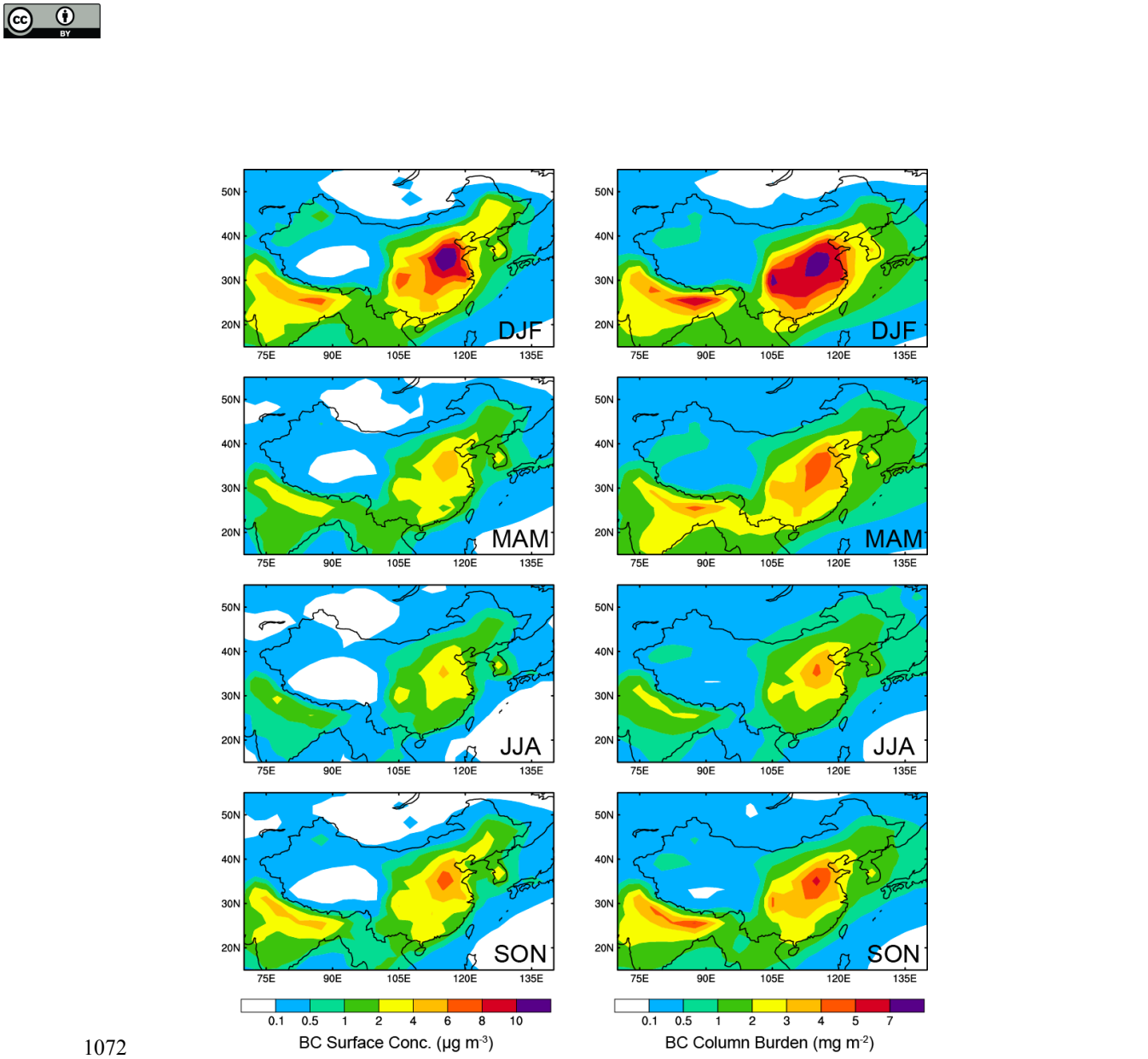

Figure 2. Simulated seasonal mean near-surface concentrations (left, units: μg m^{-3}) and column burden (right, units: mg m^{-2}) of BC in December-January-February (DJF), March-April-May (MAM), June-July-August (JJA), and September-October-November (SON).

Atmos. Chem. Phys. Discuss., doi:10.5194/acp-2016-1032, 2016
Manuscript under review for journal Atmos. Chem. Phys.
Published: 29 November 2016

Atmospheric Chemistry and Physics Discussions

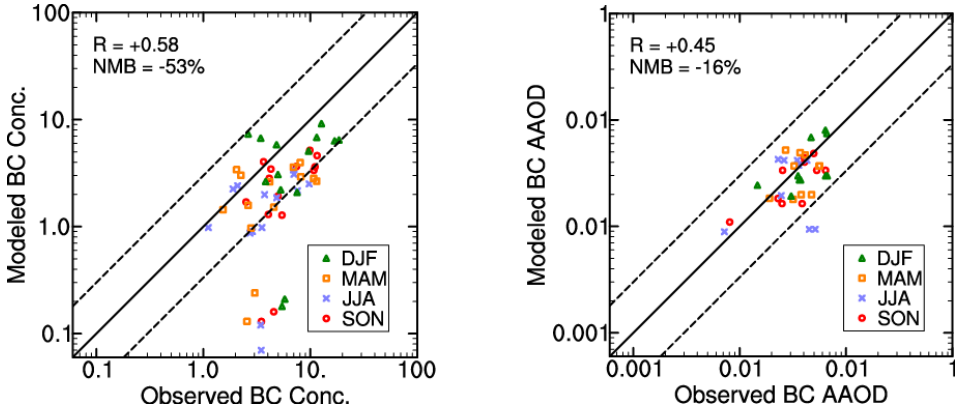

Figure 3. Comparisons of observed and modeled seasonal mean (a) near-surface concentrations (units: μg m^{-3}) and (b) aerosol absorption optical depth (AAOD) of BC in China. Solid lines mark the 1:1 ratios and dashed lines mark the 1:3 and 3:1 ratios. Observed BC concentrations were taken between 2006 and 2007 at 14 sites of the China Meteorological Administration (CMA) Atmosphere Watch Network (CAWNET) (Zhang et al., 2012). Observed AAOD of BC are obtained by removing dust AAOD from total AAOD at 10 sites of the Aerosol Robotic Network (AERONET) (Holben et al., 2001), following Bond et al. (2013). The observed AAOD are averaged over years of 2010–2014 over 7 sites and 2005–2010 over 3 sites with data available. Correlation coefficient (R) and normalized mean bias (NMB) between observation and simulation are shown on top left of each panel. NMB = $100\% \times \sum(M_i - O_i) / \sum O_i$, where M_i and O_i are the modeled and observed values at site i, respectively. Site locations are shown in Figure S1a.

Atmos. Chem. Phys. Discuss., doi:10.5194/acp-2016-1032, 2016
Manuscript under review for journal Atmos. Chem. Phys.
Published: 29 November 2016

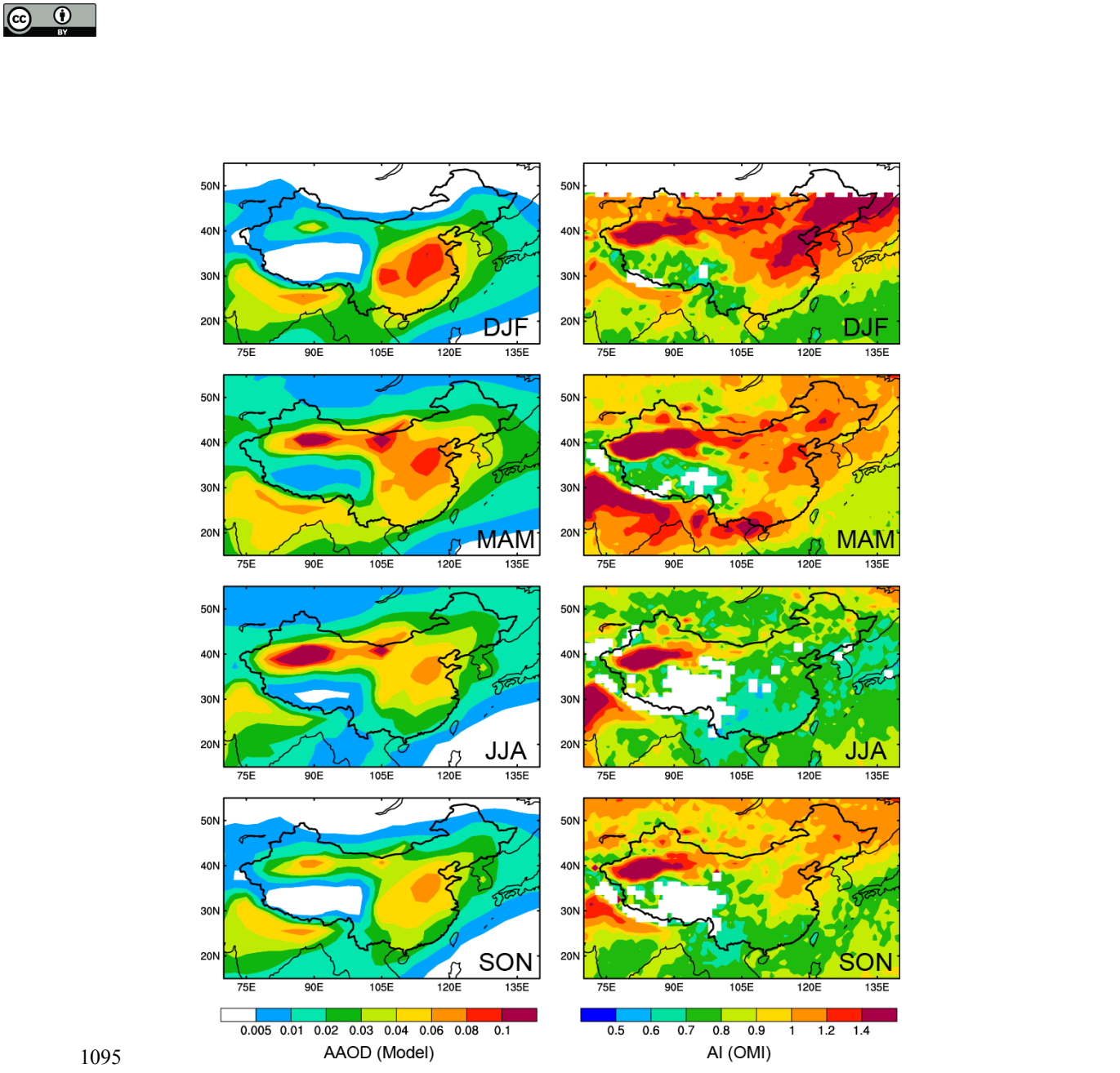

Figure 4. Spatial distribution of seasonal mean AAOD of total aerosols (left) and Aerosol Index (AI) derived from Ozone Monitoring Instrument (OMI) measurements over years of 2010–2014 (right).

Atmos. Chem. Phys. Discuss., doi:10.5194/acp-2016-1032, 2016
Manuscript under review for journal Atmos. Chem. Phys.
Published: 29 November 2016

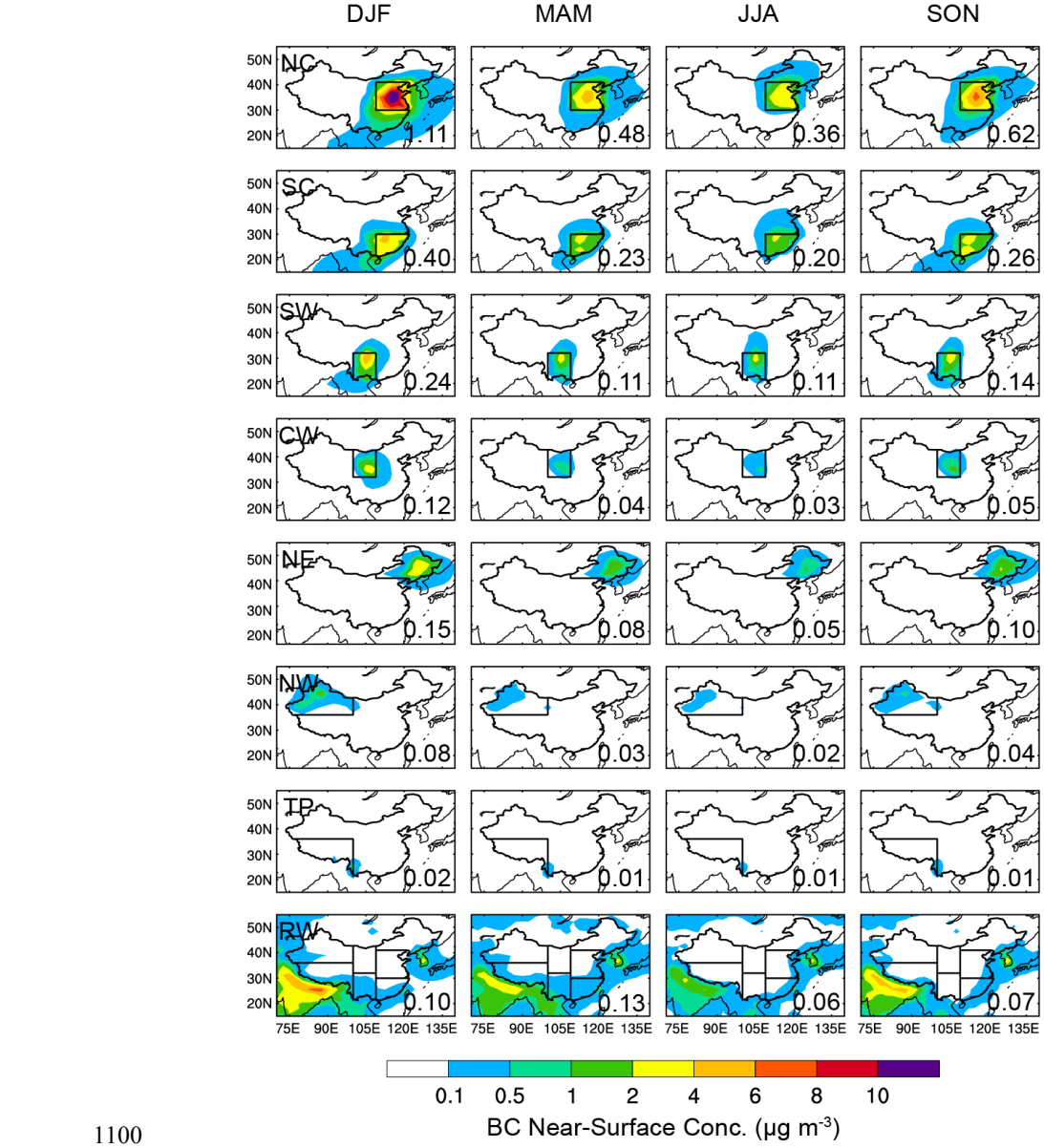

Figure 5. Spatial distribution of seasonal mean near-surface concentrations of BC (μg m^{-3}) originating from the seven source regions in China (NC, SC, SW, CW, NE, NW, and TP), marked with black outlines, and sources outside China (RW). Regionally averaged BC in China contributed by individual source regions is shown at the bottom right of each panel.

Atmos. Chem. Phys. Discuss., doi:10.5194/acp-2016-1032, 2016
Manuscript under review for journal Atmos. Chem. Phys.
Published: 29 November 2016

Atmospheric Chemistry and Physics Discussions

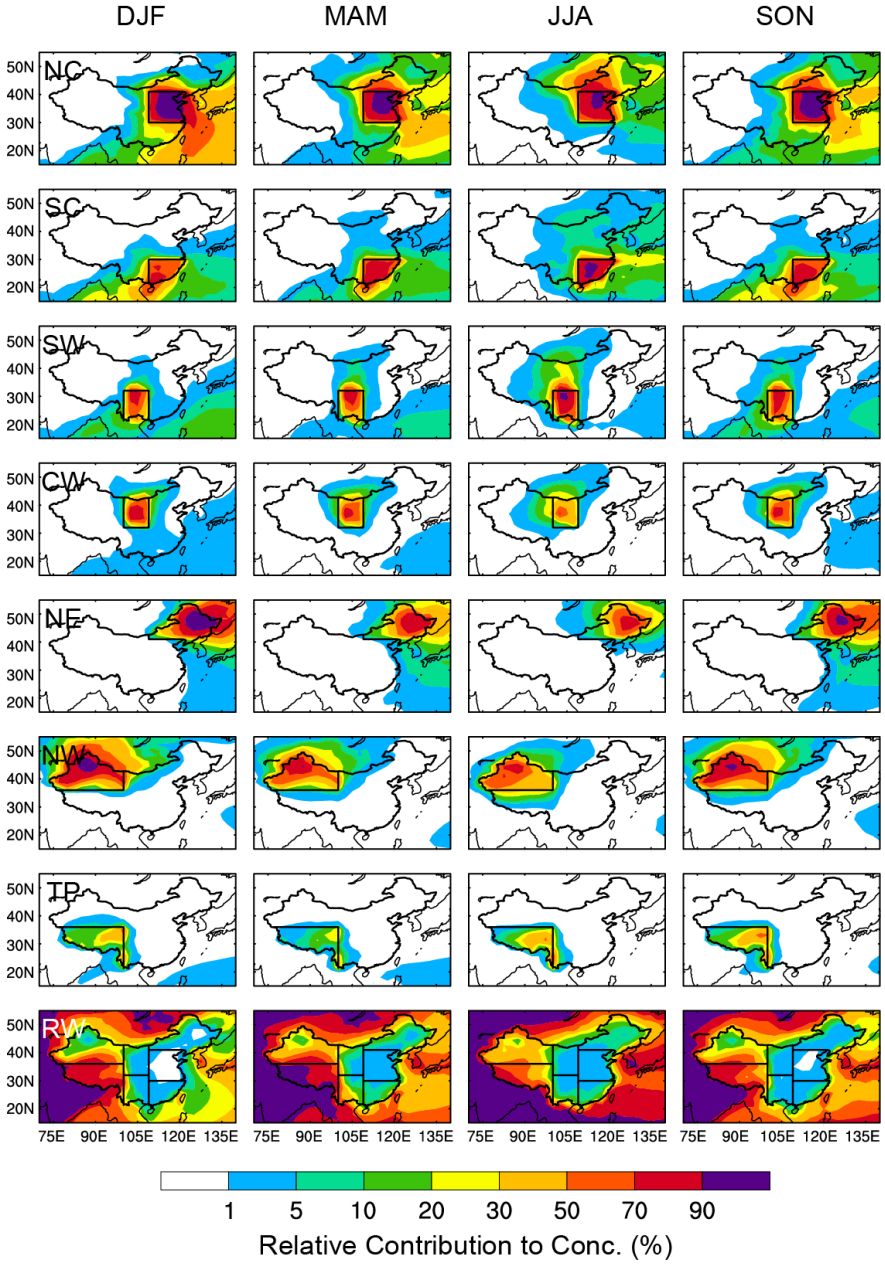

Figure 6. Spatial distribution of relative contributions (%) to seasonal mean near-surface BC concentrations from each of the tagged source regions.

Atmos. Chem. Phys. Discuss., doi:10.5194/acp-2016-1032, 2016
Manuscript under review for journal Atmos. Chem. Phys.
Published: 29 November 2016

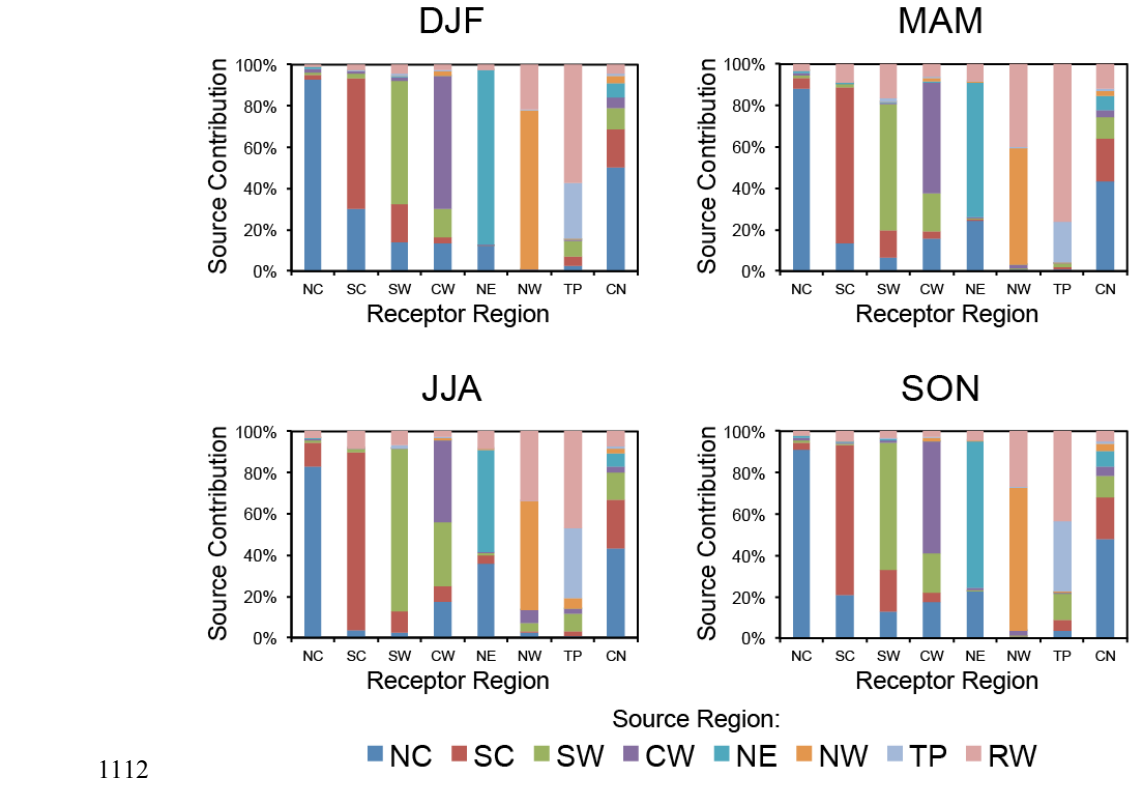

Figure 7. Relative contributions (%) from the tagged source regions (denoted by colors) to regional mean surface concentrations of BC over seven receptor regions in China (NC, SC, SW, CW, NE, NW, and TP) and China (seven regions combined, CN) in different seasons. The receptor regions are marked on the horizontal axis in each panel.

Atmos. Chem. Phys. Discuss., doi:10.5194/acp-2016-1032, 2016
Manuscript under review for journal Atmos. Chem. Phys.
Published: 29 November 2016

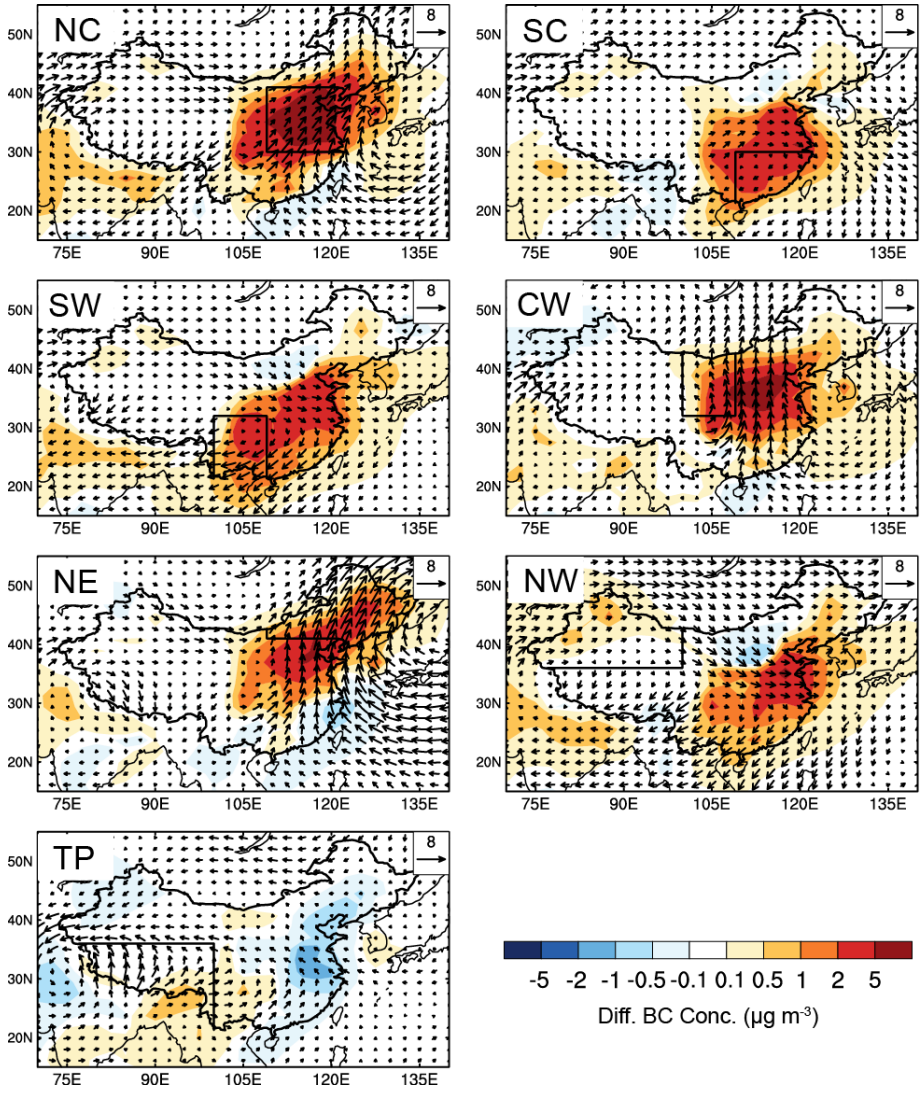

Figure 8. Composite differences in winds at 850 hPa (m s^{-1}) and near-surface BC concentrations (μg m^{-3}) between polluted and normal days in DJF.

Atmos. Chem. Phys. Discuss., doi:10.5194/acp-2016-1032, 2016
Manuscript under review for journal Atmos. Chem. Phys.
Published: 29 November 2016

Atmospheric Chemistry and Physics Discussions

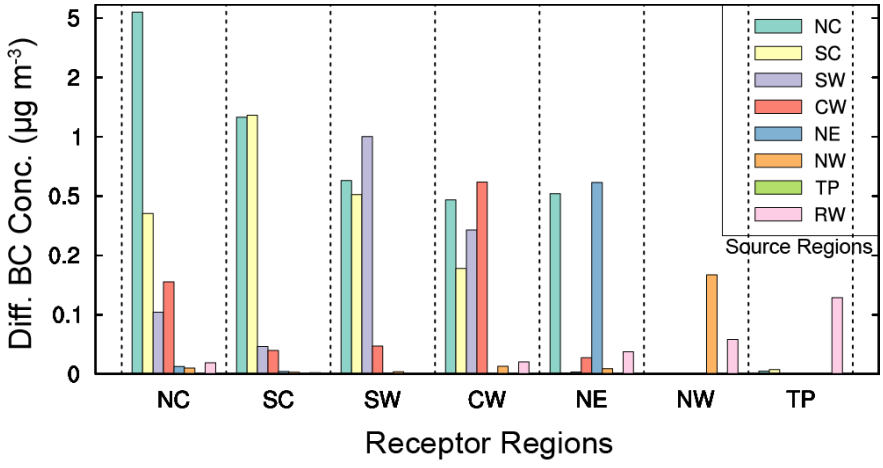

Figure 9. Composite differences in surface BC concentrations (μg m^{-3}) averaged over receptor regions (marked on the horizontal axis) over eastern and central China between polluted and normal days in DJF originating from individual sources regions (bars in each column).

Atmos. Chem. Phys. Discuss., doi:10.5194/acp-2016-1032, 2016
Manuscript under review for journal Atmos. Chem. Phys.
Published: 29 November 2016

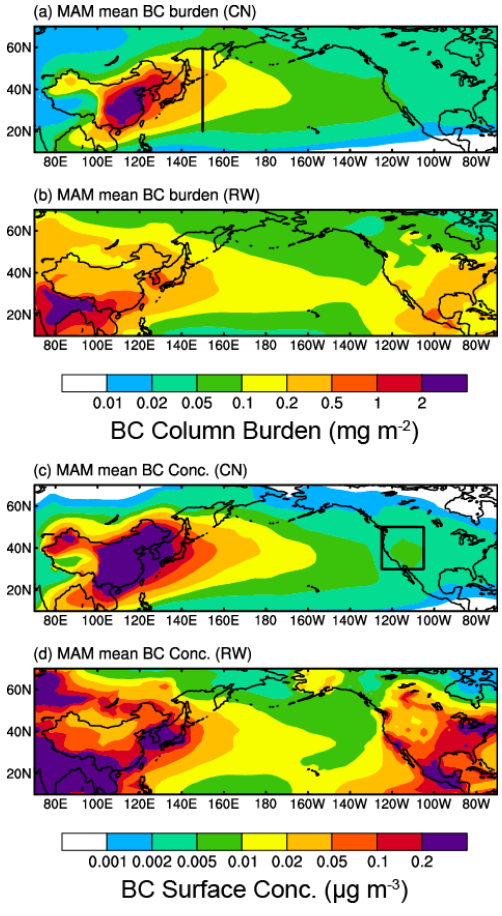

Figure 10. Spatial distribution of (a, b) column burden (mg m^{-2}) and (c, d) near-surface concentrations (μg m^{-3}) of BC originating from total emissions inside (CN) and outside China (RW), respectively, in March-April-May (MAM). The black solid lines over western (150°E, 20°–60°N) Pacific in panel (a) mark the cross-sections used to quantify outflow of BC from East Asia. The box over western United States (125°–105°W, 30°–50°N) in panel (c) is used to quantify BC concentrations attributed to sources from China.

Atmos. Chem. Phys. Discuss., doi:10.5194/acp-2016-1032, 2016
Manuscript under review for journal Atmos. Chem. Phys.
Published: 29 November 2016

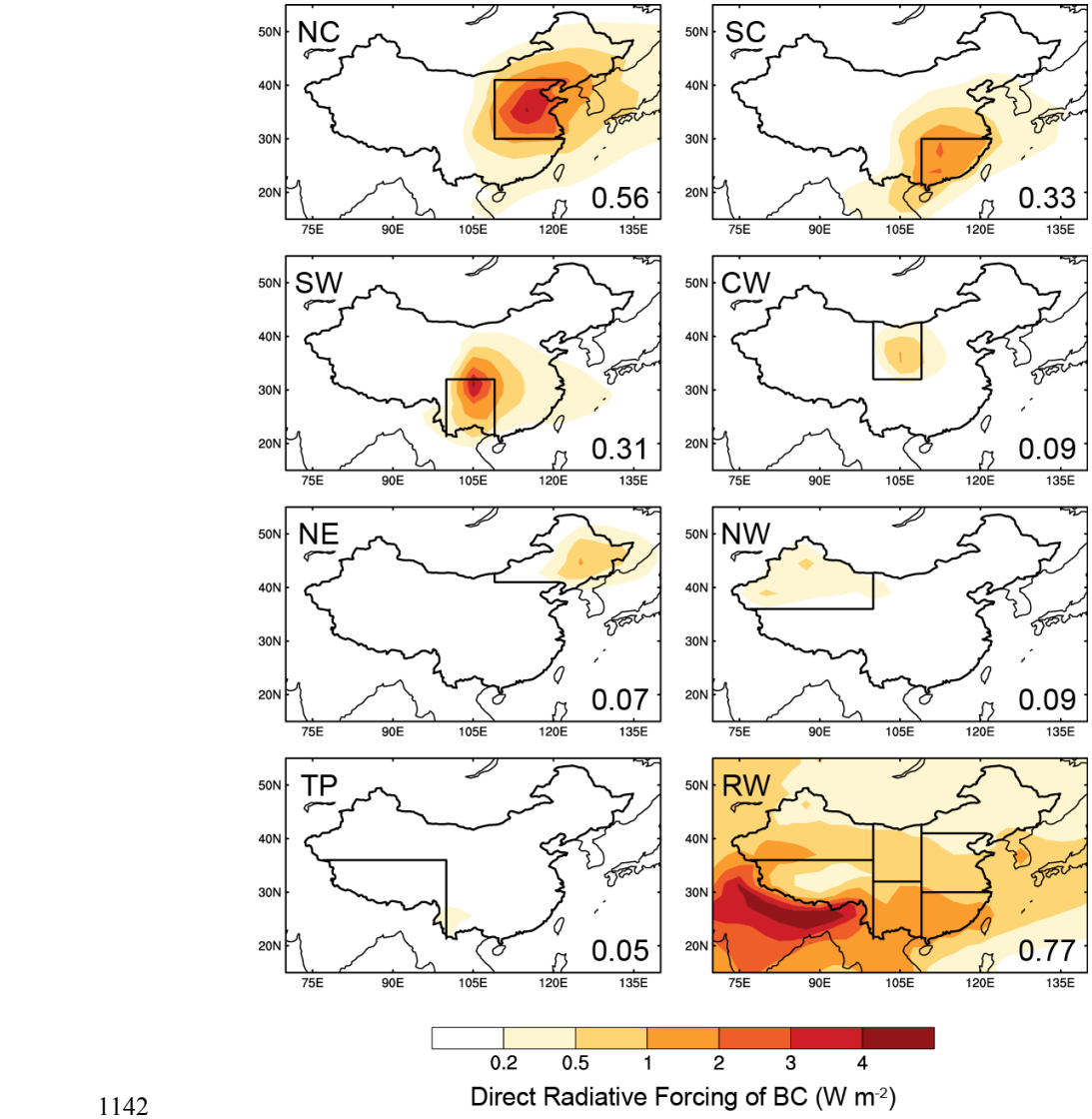

Figure 11. Spatial distribution of annual mean direct radiative forcing (DRF) of BC (W m^{-2}) at the top of the atmosphere originating from the tagged BC source regions in China (NC, SC, SW, CW, NE, NW, and TP) and source outside China (RW). Regionally averaged forcing in China contributed by individual source regions is shown at the bottom right of each panel.

Atmos. Chem. Phys. Discuss., doi:10.5194/acp-2016-1032, 2016
Manuscript under review for journal Atmos. Chem. Phys.
Published: 29 November 2016

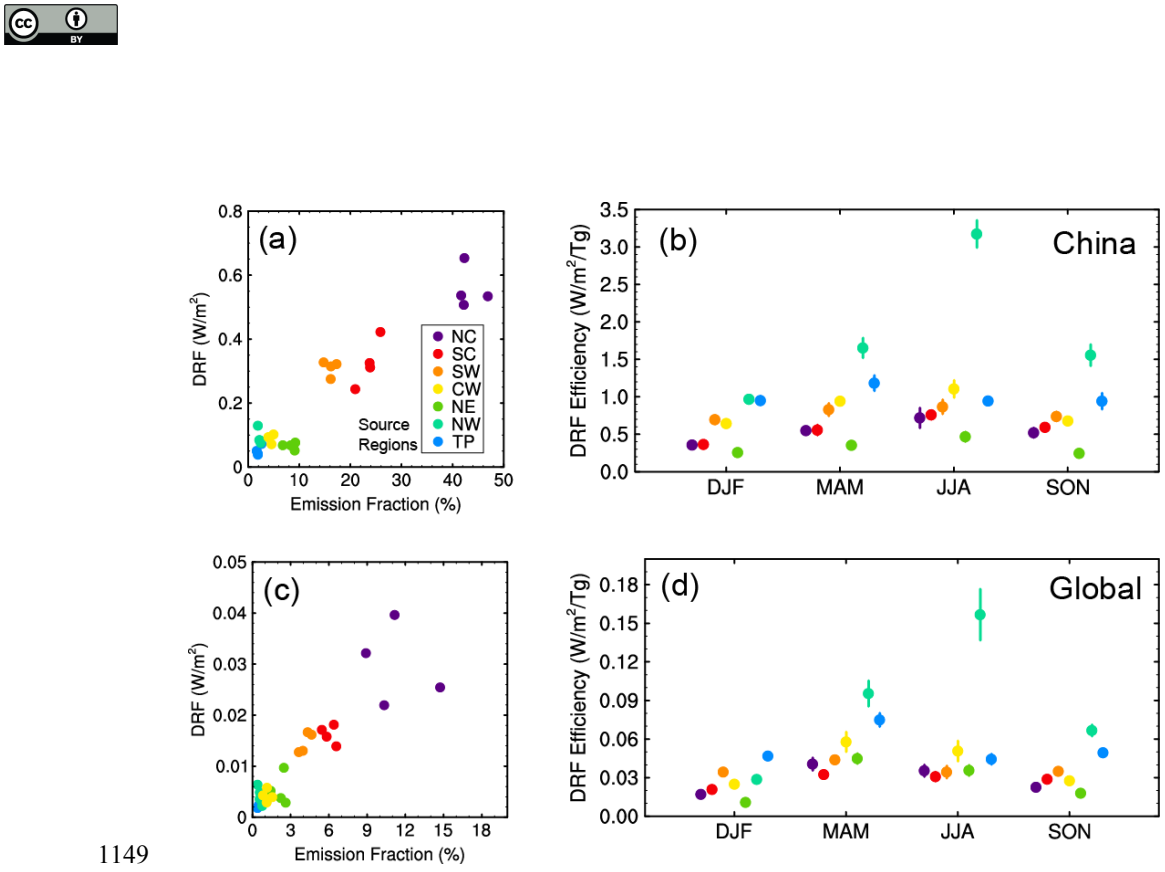

Figure 12. (a, c) BC seasonal DRF averaged over China as a function of BC emission fraction (the ratio of regional emission to the total emission over China and global, respectively, unit: %) for each of the tagged regions. (b, d) Seasonal DRF efficiency of BC (W m^{-2} Tg^{-1}) for each of the tagged source regions over China and globally, respectively. The efficiency is defined as the DRF divided by the corresponding scaled annual emission (seasonal emission multiplied by 4). Error bars indicate 1-σ of mean values during years 2010–2014.

Atmos. Chem. Phys. Discuss., doi:10.5194/acp-2016-1032, 2016
Manuscript under review for journal Atmos. Chem. Phys.
Published: 29 November 2016

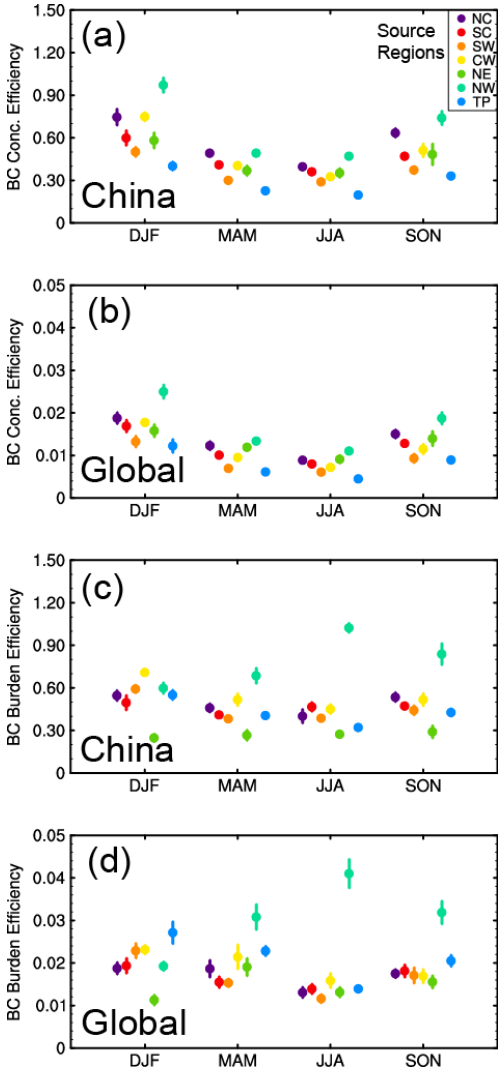

Figure 13. Seasonal (a, b) near-surface concentration (μg m^{-3} Tg^{-1}) and (c, d) column burden (mg m^{-2} Tg^{-1}) efficiency of BC for each of the tagged source regions over China and globally, respectively.